Int J Earth Sci (Geol Rundsch) (2017) 106:1919–1942
DOI 10.1007/s00531-016-1396-y

ORIGINAL PAPER

Record of Permian–Early Triassic continental arc magmatism in the western margin of the Jiamusi Block, NE China: petrogenesis and implications for Paleo-Pacific subduction

Hao Yang[1] · Wenchun Ge[1] · Yu Dong[1] · Junhui Bi[1] · Zhihui Wang[1] · Zheng Ji[1] · H. Yang[1] · W. C. Ge[1] · Y. Dong[1] · J. H. Bi[1] · Z. H. Wang[1] · Z. Ji[1]

Received: 1 April 2016 / Accepted: 31 August 2016 / Published online: 20 September 2016

Abstract In this paper, we report zircon U–Pb ages, Hf isotopes and whole-rock geochemical data for the Permian to Early Triassic granitoids from the western margin of the Jiamusi Block (WJB), NE China. The intermediate to felsic (SiO_2 = 59.67–74.04 wt%) granitoids belong to calc-alkaline series and are characterized by enrichments in light rare earth elements and large ion lithophile elements with pronounced negative Nb, Ta and Ti anomalies, revealing typical continental magmatic arc geochemical signatures. The zircon U–Pb determinations on the granodiorite, monzogranite, syenogranite and quartz diorite samples yielded ages between ca. 275–245 Ma, which, together with the published coeval intrusive rocks, indicates that Permian to Early Triassic continental arc magmatism occurred extensively in the WJB. The low and mainly negative zircon $\varepsilon_{Hf}(t)$ values between −7.6 and +1.6 and the zircon Hf model ages of 1.2–1.8 Ga, which are significantly older than their crystallization ages, suggest that they were mainly derived from reworking of ancient crustal materials with a limited input of juvenile components. The geochemical systematics and petrogenetic considerations indicate that the studied granitoids were generated from a zone of melting, assimilation, storage, and homogenization, i.e., a MASHed zone at the base of Paleo- to Mesoproterozoic continental crust, where large portions of igneous rocks and minor clay-poor sediments involved in the source region. In combination with regional geological data, we argue that the Jiamusi Block was unlikely the rifted segment of the Songliao Block and two possible geodynamical models were proposed to interpret the formation of the ca. 275–245 Ma granitoids in the WJB. In the context of Permian global plate reconstruction, we suggest that Paleo-Pacific plate subduction was initiated in the Permian to Early Triassic beneath the Jiamusi Block, and even whole eastern NE China.

Keywords Eastern NE China · Western margin of the Jiamusi Block · Permian–Early Triassic magmatism · Continental arc · Paleo-Pacific Ocean

Introduction

The Central Asian Orogenic Belt (CAOB) is one of the largest and most complex accretionary collages. This huge accretionary collage has a long strike length and evolutionary history that make it a natural laboratory to unravel geodynamic processes during accretionary orogenesis and continental growth (Kovalenko et al. 2004; Xiao et al. 2004; Windley et al. 2007; Safonova et al. 2011; Kröner et al. 2014). NE China is located in the easternmost segment of the CAOB where several microcontinental blocks have been recognized (Fig. 1). The western part, including the Erguna, Xing'an and Songliao blocks (Fig. 1), marks the broad collision zone between the North China and Siberia cratons involving the formation of multi-arc systems and accretionary complexes during subduction of the Paleo-Asian oceanic slab (Windley et al. 2007; Safonova et al. 2009; Lehmann et al. 2010). The eastern part includes the Nadanhada Terrane (Fig. 1), which, together with the Sikhote-Alin Terrane of the Russian Far East and the

Electronic supplementary material The online version of this article (doi:10.1007/s00531-016-1396-y) contains supplementary material, which is available to authorized users.

✉ W. C. Ge
gewenchun@jlu.edu.cn

[1] College of Earth Sciences, Jilin University, Changchun 130061, China

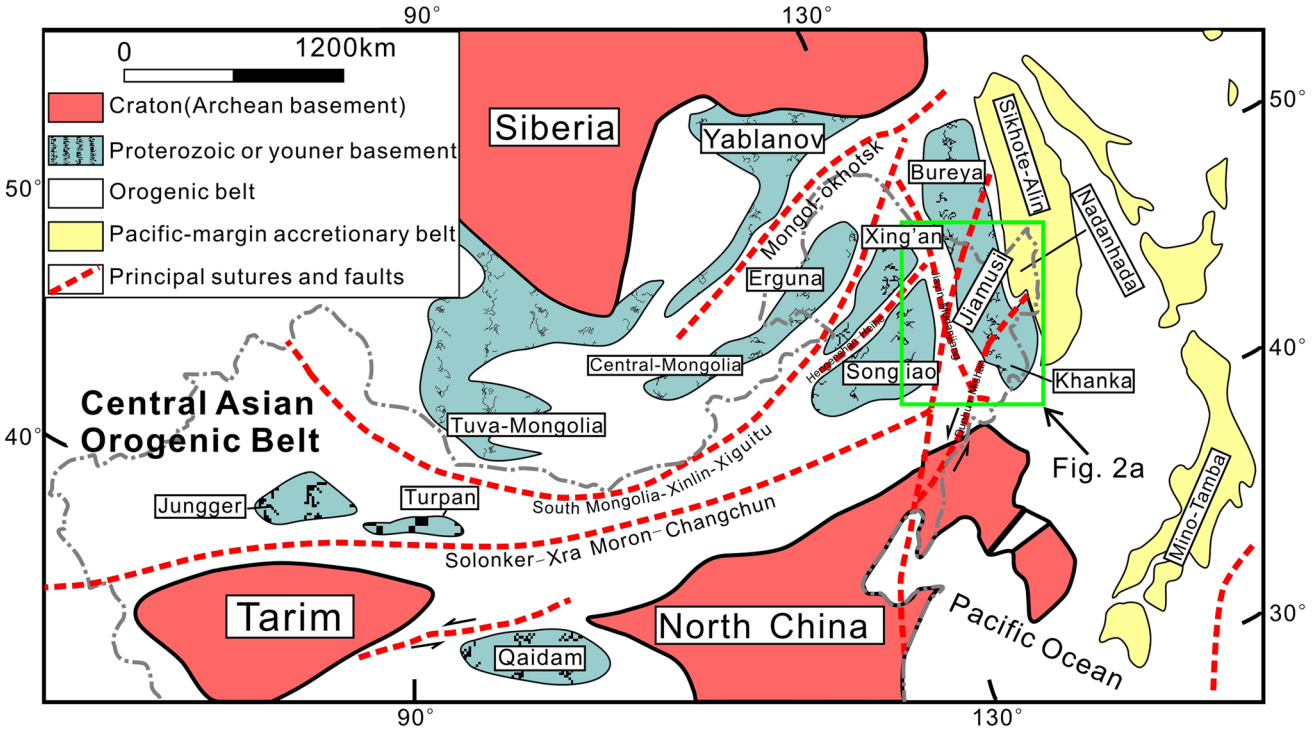

Fig. 1 Schematic diagram showing main tectonic subdivisions of central and eastern Asia (modified from Li 2006)

Japanese islands, belongs to the Paleo-Pacific margin and is characterized by late Paleozoic to early Mesozoic subduction complexes, large-scale NE-trending granite and volcanic belts, and wrench fault systems (Cheng et al. 2006; Wu et al. 2007; Zhou et al. 2009, 2014; Ge et al. 2015; Sun et al. 2015a, b). Between them is the Jiamusi-Khanka Block, it is a key area for understanding the origin of Pan-African metamorphic crustal fragments (e.g. Wilde et al. 1999, 2000, 2003, 2010; Yang et al. 2014, 2015a, b), and the processes of subduction-accretion since late Paleozoic (Yu et al. 2013a; Bi et al. 2015; Sun et al. 2015a; Yang et al. 2015a, b), although its tectonic affinity has remained controversial so far.

In the past decades, numerous researchers have been reported on the structural, petrological, geochronological and geochemical investigations on the Jiamusi-Khanka Block, and large amounts of new data have been reported on the ages, origins and tectonic settings of the Mashan Complex, Heilongjiang Complex and widespread Early Cambrian to Late Triassic igneous rocks (e.g. Wilde et al. 1999, 2000, 2003, 2010; Wu et al. 2001; Yang et al. 2012, 2014, 2015a, b). However, various and competing tectonic models proposed for the evolution of the Jiamusi-Khanka Block are still tentative and have not been fully evaluated. This is particularly the case with the late Paleozoic to early Mesozoic subduction/accretion history of the western Jiamusi Block, of which, there is an ongoing debate on the relationships between the Jiamusi and Songliao blocks. One hypothesis suggests that the Jiamusi Block rifted from the Songliao Block at some times during the Middle to Late Permian (275–258 Ma) (Zhou et al. 2009; Zhu et al. 2015), and their subsequent suturing along a N–S-trending belt defined by the Heilongjiang Complex occurred through the Late Triassic to Early Jurassic (Zhou et al. 2009, 2010) or after the Late Jurassic (Zhu et al. 2015, 2016), whereas others consider that the Jiamusi Block was an exotic block possibly derived from Gondwana (e.g. Wilde et al. 1999, 2003; Wu et al. 2011; Yang et al. 2015a), and its amalgamation with the Songliao Block along the Heilongjiang Complex did not happen until the Early Jurassic (Wu et al. 2007, 2011; Ge et al. 2015). At the western margin of the Jiamusi Block (WJB) lie vast late Paleozoic to early Mesozoic granitoids, which are geographically closely associated with the Heilongjiang Complex and show similar features of arc rock. Therefore, they could provide valuable constraints on the evolution of the Jiamusi Block. Unfortunately, few of these plutonic rocks have been comprehensively studied using the modern analysis methods, which has hindered our understanding of the tectonic settings and origins of the granitic magmas. In addition, due to poor constraints on the spatial and temporal distribution of the arc-related intrusive rocks, it is difficult to determine which oceanic subduction was responsible for the late Paleozoic to early Mesozoic tectonic evolution of the eastern NE China.

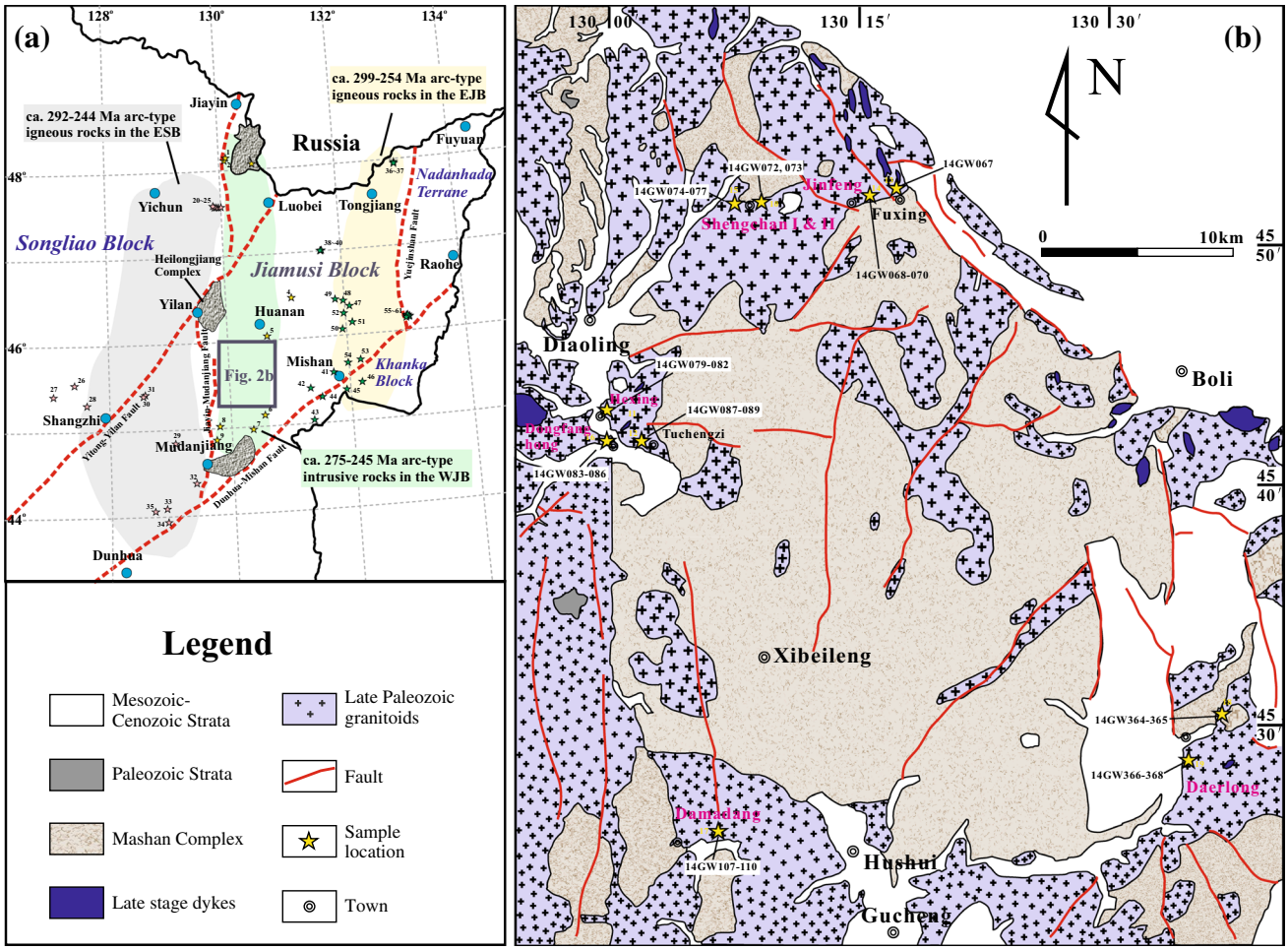

Fig. 2 **a** Sketch map of eastern Heilongjiang Province showing location of Permian–Earliest Triassic arc-type igneous rocks and Heilongjiang Complex (numbers as in Table 2) and **b** a detailed geological map of the Gucheng-Boli region showing sample location (after HBGMR 1993)

In this study, we report detailed field, petrological, LA-ICP-MS U–Pb zircon geochronological, whole-rock geochemical and zircon Hf isotopic data for the Permian–Early Triassic granitoids in the WJB, and compare these with coeval arc-type igneous rocks of the surrounding areas. Our results and conclusions provide further insight into the tectonic affinity of the Jiamusi Block and contribute to understanding the early stages of subduction processes in the eastern NE China as well as their possible links with Paleo-Pacific Ocean.

Geological setting and sample descriptions

Regional context

The CAOB is bounded by the Siberia Craton to the north, the East European Craton to the west, and the Tarim and North China cratons to the south (Fig. 1), and is generally thought to have evolved from the latest Mesoproterozoic to the late Paleozoic (Kröner et al. 2007, 2014; Safonova and Santosh 2014). NE China, part of the eastern CAOB, is considered to have formed by the amalgamation of several microcontinents, including the Erguna and Xing'an blocks in the northwest, the Songliao Block in the central part and the Jiamusi-Khanka Block and Nadanhada Terrane in the east, which are bounded to each other by deep faults (Figs. 1, 2a; Wu et al. 2007).

The Jiamusi Block is believed to extend northward into the Bureya Block and eastward into the Khanka Block in the Russian Far East and has been referred to as the Khanka–Jiamusi–Bureya block (Cao et al. 1992; Wu et al. 2007; Wilde et al. 2010; Zhou et al. 2010; Yang et al. 2014, 2015a). It comprises two different rock series: the Mashan Complex and various stages of igneous rocks. The Mashan Complex is composed dominantly of sedimentary rocks and minor volcanic rocks. It was metamorphosed in amphibolite- to granulite-facies characterized by a tight clockwise

P–T path (Jiang 1992; Lennon et al. 1997), with peak temperatures and pressures up to 850 °C and 7.4 kb, respectively (Jiang 1992). Precise zircon U–Pb ages indicate that the granulite facies metamorphism occurred at ca. 500 Ma and that detrital zircons were no older than ca. 1100 Ma (Wilde et al. 1999, 2000; Zhou and Wilde 2013). However, Ren et al. (2012) questioned this viewpoint and argued that the granulite facies metamorphism should have occurred at some time earlier than the formation of anhydrous anatectic granitoids (i.e., ca. 530 Ma). The intrusive rocks in the Jiamusi Block are divided into two phases: firstly, the early Paleozoic (540–484 Ma) intrusions that form tectonic sheets dismembering the Mashan supracrustals are associated with the Late Pan-African orogeny (Bi et al. 2014a; Yang et al. 2014); secondly, the undeformed Permian (299–254 Ma) intrusions are widespread and were emplaced in an active continental margin setting (Wu et al. 2001, 2011; Yu et al. 2013a, b; Bi et al. 2014b, 2015; Sun et al. 2015a; Yang et al. 2015a). These Phanerozoic intrusions, together with widespread volcanic rocks (Meng et al. 2008), make up much of the Jiamusi Block. The Khanka Block occurs mainly in Far East Russia with only a small segment cropping out in NE China. The metamorphic rocks of the Russian part of the Khanka Block yield an age for the protolith of 757 ± 4 Ma, and the age of peak metamorphism is 506.9 ± 2.6 Ma (Khanchuk et al. 2010). The granitoids in the Chinese part of the Khanka Block formed in the early Paleozoic orogeny collapse stage, in a Permian active continental margin setting, and in a Late Triassic extensional environment (Wilde et al. 2003; Yang et al. 2012, 2015a, b; Wang et al. 2015).

Lying west of the Jiamusi Block is the Songliao Block that consists of the Mesozoic Songliao Basin, the Lesser Xing'an Range, and the Zhangguangcai Range. The Lesser Xing'an and Zhangguangcai Ranges are characterized by voluminous Phanerozoic granitoids along with rare Paleozoic strata (Wu et al. 2002). The Phanerozoic granitoids are composed mainly of syn-collisional Mesozoic granitic rocks, interpreted to result from westward subduction of the Jiamusi beneath the Songliao block between 216 ± 4 and 184 ± 4 Ma (Wu et al. 2002, 2007). Data from several hundred drill holes of the Songliao Basin reveal that Paleozoic–Mesozoic granitoids and Paleozoic strata (Gao et al. 2007; Pei et al. 2007) are widespread in the basement, with minor Precambrian components (Wang et al. 2006; Pei et al. 2007) that may represent a tectonic slice of the North China Craton (Wu et al. 2011).

Intervening between the Jiamusi and Songliao blocks is the Heilongjiang Complex that is exposed along the Jiayin–Mudanjiang Fault, extending from Luobei in the north, through Yilan in the central, to Mudanjiang in the south (Fig. 2a). The Heilongjiang Complex is composed mainly of serpentinite, glaucophane-bearing metabasalt, greenschist, marble, quartz-schist, two mica-schists, and quartzite (Wu et al. 2007). The rocks were metamorphosed in the epidote–blueschist facies, with *P–T* conditions of 0.9–1.1 GPa and 320–450 °C, respectively (Zhou et al. 2009). Field observations show that the Heilongjiang Complex is structurally interleaved with the Mashan Complex (Cao et al. 1992; Wu et al. 2007). It has been considered to be an accretionary complex with suturing at ca. 185 Ma, related to Paleo-Pacific Ocean subduction (Wu et al. 2007; Zhou et al. 2009). Most recently, however, Zhu et al. (2015) reported that the basaltic protoliths of some blueschists from the Heilongjiang Complex formed at ~142 Ma, suggesting the suturing must have happened at some time after ~142 Ma.

The Yuejinshan accretionary complex, trending NE–SW between the Jiamusi Massif and the Nadanhada Terrane, is composed of a metamorphic mélange and ultramafic–mafic rocks. The mélange consists of upper greenschist facies mica-schist, phengite-schist, quartz-schist, marble, and mafic–ultramafic igneous rocks. The ultramafic–mafic rock association consists of oceanic meta-ultramafic–mafic volcanic and intrusive rocks, including meta-peridotite, pyroxenite (layered) gabbro, diorite and basalt. Yang et al. (1998) reported a whole-rock Rb–Sr isochron age of 188 ± 4 Ma for greenschist in the Dongfanghong area. Zhang et al. (1997) and Zhou et al. (2014) identified MORB-type metabasalt from the Yuejinshan Complex. More recently, the Permian (290–274 Ma) Dongfanghong gabbro has also been recognized, and geochemical data suggest that they formed in an immature island arc (Sun et al. 2015a) or a continental arc (Bi et al. 2015), possibly related to subduction of the Paleo-Pacific Plate beneath the Jiamusi Block (Sun et al. 2015a; Yang et al. 2015a). Due to a lack of comprehensive and detailed studies, the architecture, geochronology, geochemistry and tectonic evolution of the Yuejinshan accretionary complex is still debated.

Field relations and petrology

The present study was carried out in the Gucheng-Boli region in the eastern Heilongjiang Province, situated within the WJB (Fig. 2a). The outcropping units include the Mashan Complex, the Heilongjiang Complex, rare Paleozoic strata, and voluminous Mesozoic to Cenozoic volcanic–sedimentary assemblages (HBGMR 1993). The intrusive rocks are widely distributed in the western Jiamusi Block (Fig. 2b; HBGMR 1993), the types of which vary from basic to acidic, most are granitoids emplaced as batholiths with only minor stocks or dikes. In this paper, we focused on nine granitic intrusions, named the Daerlong, Damadang, Dongfanghong, Shengchan II, Jinfeng, Fuxing, Tuchengzi, Hexing and Shengchan I plutons (Fig. 2b). The geological boundaries between the plutons are uncertain

as the region is heavily forested. Their field relations, rock associations and petrographic features are summarized in Table 1, and representative photographs of the samples are shown in Fig. 3.

Analytical methods

Zircon U–Pb dating by LA-ICP-MS

Zircons from ten sample analyzed in this study were extracted from whole-rock samples by using combined magnetic and heavy liquid separation at the Langfang Regional Geological Survey, Hebei Province, China. Recovered zircon grains together with chips of zircon standards Qinghu were mounted in epoxy disks and polished to expose the longitudinal section of crystals for analysis. All zircons were then examined under transmitted and reflected light with an optical microscope. Cathodoluminescence (CL) images were collected using a CL spectrometer (Garton Mono CL3+) equipped on a Quanta 200F ESEM with 2-min scanning time at conditions of 15 kV and 120 nA. Distinct domains within the zircons were selected for analysis based on transmitted and reflected light micrographs as well as CL images. Samples were analyzed for U–Pb geochronology on an Agilent 7500 inductively coupled plasma–mass spectrometer (ICP–MS) equipped with a 193 nm laser system at the Institute of Geology and Geophysics, Chinese Academy of Sciences, Beijing, China. The diameter of the laser spot was 32 μm throughout the analyses, and the ablation rate was 10 Hz. Zircon 91500 was used as the external standard and a standard silicate glass (Nist 610) was used to optimize the instrument. Isotopic ratios and element contents were calculated using the Glitter program (ver. 4.4, Macquarie University). Common Pb was corrected following Andersen (2002). The age calculations and concordia plots were made using Isoplot (ver. 3.0) (Ludwig 2003).

Lu–Hf isotope analysis

Eight of the dated samples were selected for the in situ zircon Hf isotopic analyses that were carried out on a Neptune multi-collector ICPMS, equipped with 193 nm laser, at the Institute of Geology and Geophysics, Chinese Academy of Sciences (Beijing), China. Hf isotopic analyses were reported with spot of 63 μm in diameter, laser repetition rate of 10 Hz, and laser beam energy density of 10 J/cm^2. The detailed analytical procedures were described by Wu et al. (2006). Isobaric interference correction for ^{176}Lu on ^{176}Hf was performed by measuring the intensity of the interference-free ^{175}Lu isotope plus a recommended ^{176}Lu/^{175}Lu ratio of 0.02655 to calculate ^{176}Lu/^{177}Hf ratios. Isobaric interference of ^{176}Yb on ^{176}Hf was corrected by measuring an interference-free ^{172}Yb isotope and using a ^{176}Lu/^{172}Yb ratio of 0.5886. The measured ^{176}Hf/^{177}Hf ratio of standard zircon 91,500 of 0.282289 ± 0.000024 is within error of the commonly accepted value of 0.282284 ± 0.000022 determined using the solution method (Griffin et al. 2006). The measured ^{176}Hf/^{177}Hf and ^{176}Lu/^{177}Hf ratios were used to calculate the initial ^{176}Hf/^{177}Hf ratios, taking the decay constant for ^{176}Lu as 1.865×10^{-11}/year (Scherer et al. 2001). The present-day chondritic ratios of ^{176}Hf/^{177}Hf = 0.282785 ± 11 and ^{176}Lu/^{177}Hf = 0.0336 ± 1 (Bouvier et al. 2008) were adopted to calculate $\varepsilon_{Hf}(t)$ values, and the solution method (Amelin et al. 2000) was used to calculate Hf model ages.

Major and trace element analysis

After petrographic examination, 30 fresh granitoid samples were selected, crushed, and powdered in an agate mill. Whole-rock chemical analyses were conducted at the Beijing Research Institute of Uranium Geology, Beijing, China. Major element analyses were made by X-ray fluorescence (XRF; AB-104L, PW2404) using fused glass disks according to Chinese national standard (GB/T14506.14-2010). Trace element concentrations were determined using an ELEMENT XR inductively coupled with plasma mass spectrometer (ICP–MS) according to Chinese national standard (GB/T14506.30-2010). The analytical results for Chinese standard rock (GDW07104) indicated that the analytical precision was better than 5 % for major elements and 10 % for trace and rare earth elements.

Analytical results

Zircon U–Pb ages and Lu–Hf isotopes

The resulting LA-ICP-MS U–Pb data of 10 granitoids are listed in Supplementary Table S1, and zircon Lu–Hf isotopic compositions of eight of the dated samples are given Supplementary Table S2. The CL images of representative zircons and age concordia plots are shown in Figs. 4 and 5.

Shengchan I pluton

Zircon grains from the granodiorite sample (14GW073) are generally euhedral and display fine-scale oscillatory zoning with occasional dark and narrow rim on CL images (Fig. 4). The ^{206}Pb/^{238}U ages given by 16 analytical zircons range from 239 to 266 Ma, defining a weighted mean age of 249 ± 4 Ma (MSWD = 2.10) (Fig. 5a), which is considered to represent the crystallization age of the granodiorite (i.e., Early Triassic).

Table 1 Geological and petrological characteristics of the Permian–Early Triassic granitoids in the western margin of the Jiamusi Block

Sample no.	Pluton	GPS location	Lithology	Texture and structure	Modal mineral (vol. %)							Field characteristics
					Q	Af	Pl	Bi	Hb	Ms'	Am	
14GW072, 073	Shengchan I	E130°09′04.8″ N45°51′54.4″	Granodiorite	Fine to medium-grained granitic texture Massive structure	30	15	45	5–8	1		3	Intrudes older granites, and overlain by Cenozoic strata
14GW079-082	Hexing	E129°59′52.2″ N45°42′54.1″	Syenogranite	Fine to medium-grained granitic texture Massive structure	40	45	10	2	1		2	Overlain by Cenozoic strata, and intruded by alkali-feldspar granite and diabase dykes
14GW087-089	Tuchengzi	E130°01′22.5″ N45°41′32.7″	Quartz diorite	Fine-grained granitic texture Massive structure	15	15	55	7	5		3	Intrudes sedimentary rocks of Mashan Complex, and overlain by Cenozoic strata
14GW067	Fuxing	E130°17′11.8″ N45°51′54.6″	Granodiorite	Fine to medium-grained granitic texture Massive structure	37	13	40	6		1	3	Overlain by Cretaceous volcanic rocks, and dioritic MEs can been found
14GW068-070	Jinfeng	E130°15′23.4″ N45°51′22.1″	Syenogranite	Fine-grained granitic texture Weak gneissic structure	30	48	15	3		<1	3	Intrudes marbles of Mashan Complex
14GW074-077	Shengchan II	E130°07′37.8″ N45°51′51.0″	Monzogranite	Fine to medium-grained granitic texture Massive structure	32	35	25	5	<1		2	Intrudes older granites, and minor dioritic MEs can been found
14GW083-086	Dongfanghong	E130°00′11.5″ N45°41′49.4″	Granodiorite	Medium-grained granitic texture Massive structure	40	43	10	5–7	1		3	Intruded by alkali-feldspar granite dyke, and minor dioritic MEs can been found
14GW107-110	Damadang	E130°06′58.7″ N45°25′10.3″	Granodiorite	Fine-grained granitic texture Massive structure	32	17	42	5	<1		3	Intrudes older granites and Mashan Complex, and minor MEs can been found
14GW364-368	Daerlong	E130°36′48.5″ N45°30′33.5″	Granodiorite	Fine to medium-grained granitic texture Massive structure	35	13	44	7	<1		2	Intruded by late stage of granite dyke, and overlain by Mesozoic and Cenozoic strata

Q quartz, *Af* alkaline feldspar, *Pl* plagioclase, *Bi* biotite, *Hb* hornblende, *Ms'* secondary muscovite, *Am* accessory mineral

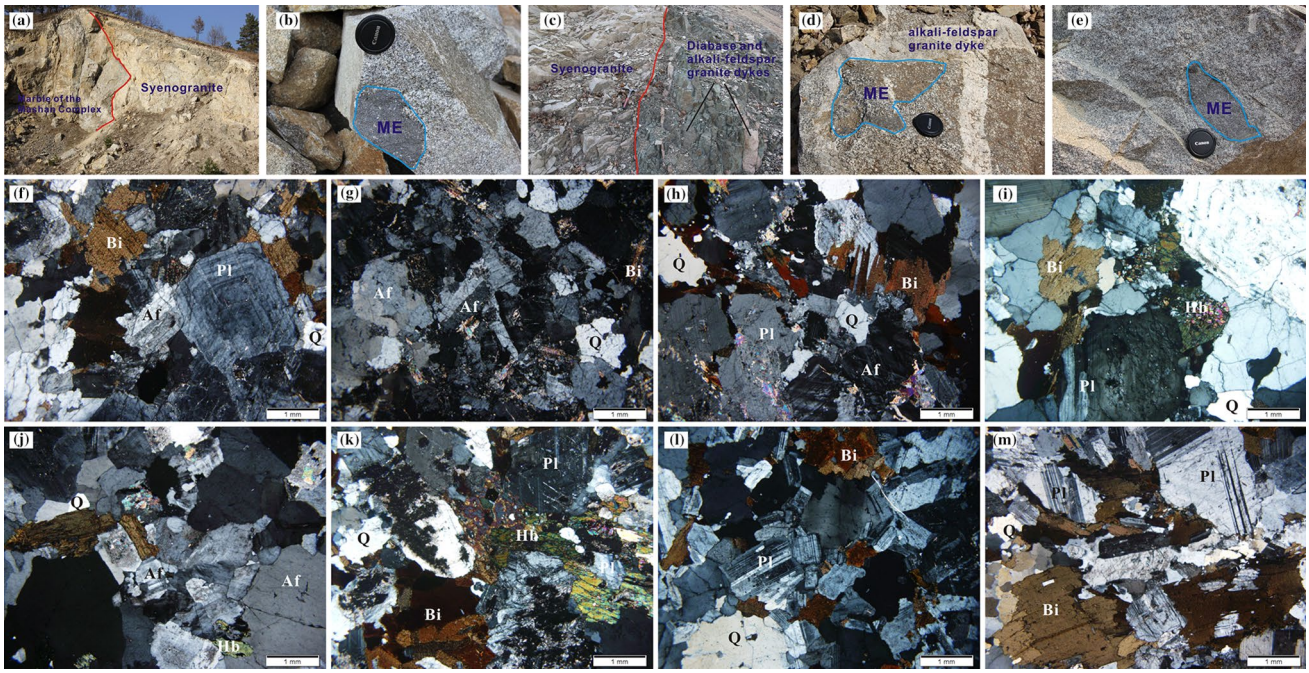

Fig. 3 Photographs and microphotographs (cross-polarized light) showing field relationships and textures. **a** Outcrop of Jinfeng syenogranite, intruding marbles of the Mashan Complex, **b** microgranular enclave (ME) locally exists in the Shengchan II monzogranite, **c** Hexing syenogranite cut by diabase and alkali-feldspar granite dykes, **d** Dongfanghong granodiorite cut by a alkali-feldspar granite dyke, and minor dioritic MEs can been found, **e** ME locally exists in the Damadang granodiorite, **f** Fuxing granodiorite (sample 14GW067), **g** Jinfeng syenogranite (sample 14GW068), **h** Shengchan II monzogranite (sample 14GW074), **i** Dongfanghong granodiorite (sample 14GW085), **j** Hexing syenogranite (sample 14GW079), **k** Tuchengzi quartz diorite (sample 14GW087), **l** Damadang granodiorite (sample 14GW107) and **m** Daerlong granodiorite (sample 14GW366). *Q* quartz, *Af* alkaline feldspar, *Pl* plagioclase, *Bi* biotite, *Hb* hornblende

Hexing pluton

Zircons separated from the syenogranite sample (14GW079) are generally euhedral to subhedral, although some are slightly rounded. Most grains are bright and show oscillatory and banded zoning, whereas the minority displays weak oscillatory zoning and dark luminescence (Fig. 4). Except for three analyses (spots 1, 4, 10) showing obvious Pb loss, the remaining 21 analyses display Th/U ratios of 0.34–0.59 and yield a concordia age group of 246 ± 2 Ma (MSWD = 0.38) (Fig. 5b), interpreted as the magmatic crystallization age of the syenogranite (i.e., Early Triassic). Twenty of the dated zircons were measured for Lu–Hf isotopes. With one exception showing $\varepsilon_{Hf}(t)$ and T_{DM2} values of −22.9 and 2719 Ma, the others exhibit relatively homogeneous Hf isotopic compositions with initial $^{176}Hf/^{177}Hf$ ratios, $\varepsilon_{Hf}(t)$, and T_{DM2} values varying from 0.281691 to 0.282329, from −4.6 to +1.6, and from 1165 to 1565 Ma, respectively (Fig. 6; Supplementary Table S2).

Tuchengzi pluton

Zircons from the quartz diorite sample (14GW088) are generally euhedral in shape with length: width ratios of 1:1–4:1. They have high Th/U ratios of 0.14–0.54 and display fine-scale oscillatory zoning (Fig. 4). The $^{206}Pb/^{238}U$ ages obtained from 24 analytical spots are in the range of 244–256 Ma, yielding a weighted mean age of 250 ± 2 Ma (MSWD = 0.60) (Fig. 5c), interpreted to represent the crystallization age of the quartz diorite (i.e., Early Triassic). Twenty analyses of the dated zircons were conducted for Lu–Hf isotopes, and their initial $^{176}Hf/^{177}Hf$ ratios range from 0.281956 to 0.282311, and $\varepsilon_{Hf}(t)$ and T_{DM2} values vary from −6.6 to −4.2, and from 1542 to 1696 Ma, respectively (Fig. 6; Supplementary Table S2).

Fuxing pluton

Zircons from the granodiorite sample (14GW067) are euhedral in shape and exhibit fine-scale oscillatory zoning (Fig. 4). A total of 24 analyses were made on 24 zircons. Excluding one spot with a discordant age and four spots with older ages (734 ± 6, 319 ± 4, 284 ± 4, and 275 ± 3 Ma), the other 19 analyses give $^{206}Pb/^{238}U$ ages of 248–263 Ma, yielding a weighted mean age of 256 ± 2 (MSWD = 1.70, Fig. 5d). The younger age (256 ± 2 Ma) is interpreted as the crystallization age of the granodiorite (i.e., Late Permian), whereas the older ones (734, 319, 284,

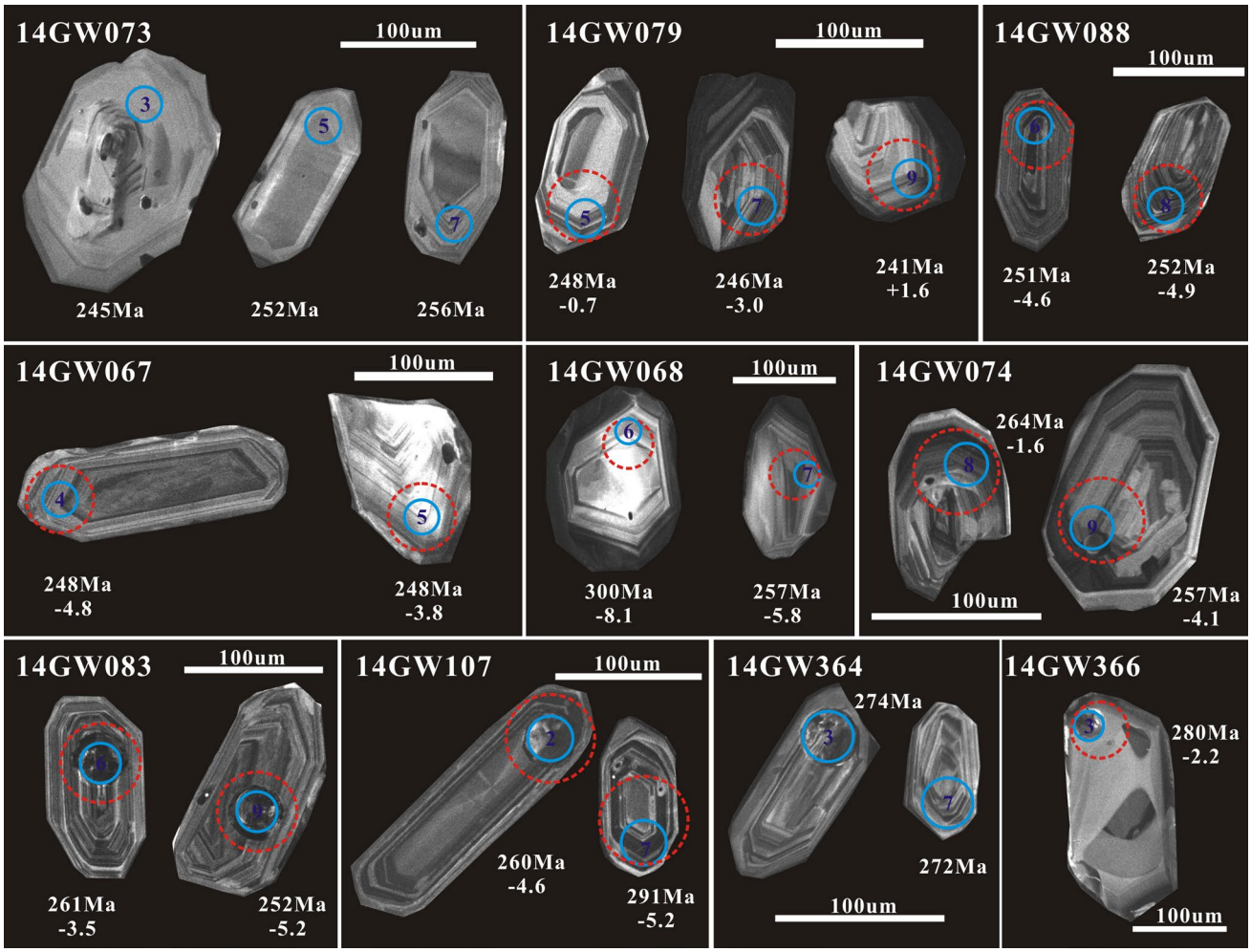

Fig. 4 Cathodoluminescence (CL) images of zircons selected from the Permian–Early Triassic granitoids in the Gucheng-Boli region. The *numbers* on these images indicate individual analysis spots, and the values below show zircon ages and $\varepsilon_{Hf}(t)$ values

and 275 Ma) represent the crystallization ages of xenocrystic zircons entrained in the granodiorite magma. Twenty of the dated zircons were analyzed for Lu–Hf isotopes, and 16 analyses with ages of ~256 Ma have initial $^{176}Hf/^{177}Hf$ ratios of 0.281972–0.282300 with $\varepsilon_{Hf}(t)$ and T_{DM2} values of −6.6 to −4.4 and 1559–1697 Ma, respectively (Fig. 6; Supplementary Table S2). The xenocrystic zircons with older ages (275–734 Ma) have $^{176}Hf/^{177}Hf$ ratios, $\varepsilon_{Hf}(t)$ and T_{DM2} values in the range of 0.281717–0.282227, −3.9 to −2.1, and 1482–1846 Ma, respectively.

Jinfeng pluton

Zircons separated from the syenogranite sample (14GW068) are prismatic and display oscillatory and banded zoning with occasional dark and narrow rim (Fig. 4). Analyses for U–Pb isotopes were conducted on 24 zircons. Fourteen analyses yield $^{206}Pb/^{238}U$ ages of 247–257 Ma, defining a concordia age group of 254 ± 2 Ma (MSWD = 0.36, Fig. 5e), which is considered as the emplacement age of this pluton (i.e., Late Permian). The remaining 10 spots give one age group at 297 ± 4 Ma (MSWD = 0.23, n = 7) and three older inherited ages of 277 ± 5 Ma, 434 ± 7 Ma, and 469 ± 7 Ma. Twenty analyses were conducted for Lu–Hf isotopes on the dated zircons. Thirteen magmatic zircons with ages of ~254 Ma have initial $^{176}Hf/^{177}Hf$ ratios of 0.282072–0.282339 with $\varepsilon_{Hf}(t)$ and T_{DM2} values of −7.6 to −5.6 and 1633–1762 Ma, respectively (Fig. 6; Supplementary Table S2).

Shengchan II pluton

Zircons from the monzogranite sample (14GW074) are prismatic in shape with fine-scale oscillatory zoning (Fig. 4). Twenty-five analyses on 25 zircons give $^{206}Pb/^{238}U$ ages ranging from 251 to 266 Ma, yielding a peak age population of 258 ± 2 Ma (MSWD = 0.95) (Fig. 5f), which is considered to represent the time of crystallization of the

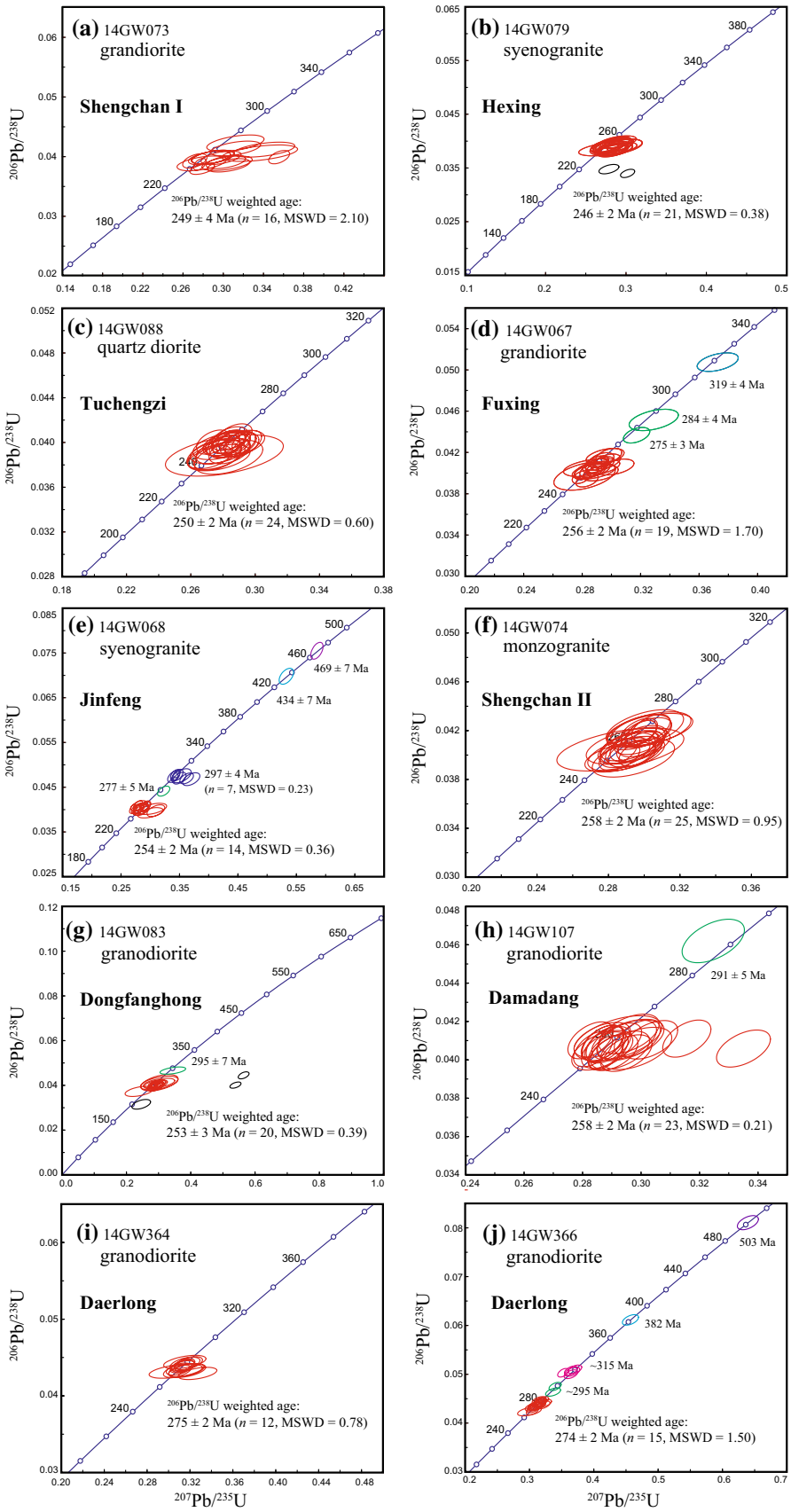

Fig. 5 Zircon LA–ICP–MS U–Pb concordia diagrams for the Permian–Early Triassic granitoids from the Gucheng-Boli region. The weighted mean age and MSWD are shown in each figure

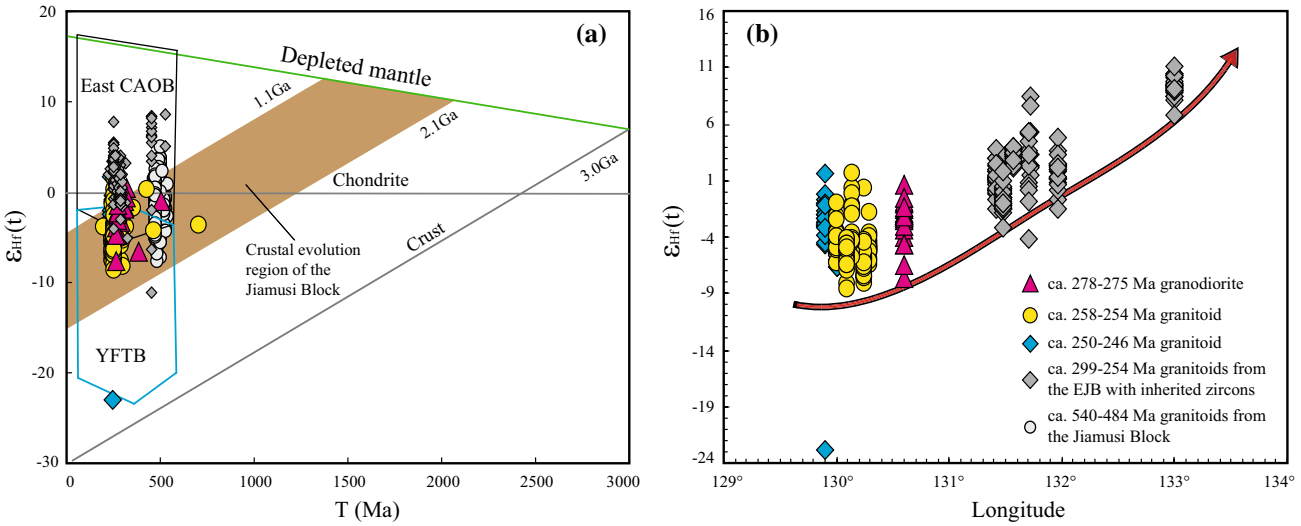

Fig. 6 **a** $\varepsilon_{Hf}(t)$ versus t diagram of the Permian–Early Triassic granitoids from the Gucheng–Boli region, also showing the ca. 299–254 Ma granitoids from the EJB (Yu et al. 2013a; Bi et al. 2014b; Yang et al. 2015a) and the ca. 540–484 Ma granitoids from the Jiamusi Block (Bi et al. 2014a; Yang et al. 2014), *YFTB* the Yanshan Fold and Thrust Belt and **b** plot of the latitude of sampling location versus values of $\varepsilon_{Hf}(t)$

monzogranite (i.e., Late Permian). Fifteen of the dated zircons were analyzed for Lu–Hf isotopes, and they have initial $^{176}Hf/^{177}Hf$ ratios of 0.281947–0.282320 with $\varepsilon_{Hf}(t)$ and T_{DM2} values of −5.8 to +1.6 and 1181–1647 Ma, respectively (Fig. 6; Supplementary Table S2).

Dongfanghong pluton

Zircons from the granodiorite sample (14GW083) are prismatic and exhibit fine-scale oscillatory zoning (Fig. 4). Twenty-four analyses were made on 24 zircons. Excluding three analyses showing obvious Pb loss and one xenocrystic zircon with an older age (295 ± 7 Ma), the remaining 20 analyses yield $^{206}Pb/^{238}U$ ages of 237–261 Ma, defining a weighted mean age of 253 ± 3 (MSWD = 0.39, Fig. 5g), interpreted as the crystallization age of the granodiorite (i.e., Late Permian). Fifteen of the dated zircons were conducted for Lu–Hf isotopes, and 14 data with ages of ~253 Ma have initial $^{176}Hf/^{177}Hf$ ratios, $\varepsilon_{Hf}(t)$ and T_{DM2} values ranging from 0.281913 to 0.282240, from −6.3 to −1.0, and from 1346 to 1675 Ma, respectively (Fig. 6; Supplementary Table S2).

Damadang pluton

Zircons from the granodiorite sample (14GW107) are euhedral in shape with length: width ratios of 3:1–5:1. They have high Th/U ratios of 0.18–0.69 and exhibit fine-scale oscillatory zoning (Fig. 4). Except for one xenocrystic zircon with an older age (291 ± 5 Ma), the remaining 23 analyses yield $^{206}Pb/^{238}U$ ages of 255–261 Ma, giving a weighted mean age of 258 ± 2 (MSWD = 0.21, Fig. 5h), which is considered as the crystallization age of the granodiorite (i.e., Late Permian). Twenty of the dated zircons were measured for Lu–Hf isotopes, and 19 analyses with ages of ~258 Ma have initial $^{176}Hf/^{177}Hf$ ratios of 0.282003–0.282256, with $\varepsilon_{Hf}(t)$ and T_{DM2} values varying from −8.7 to −4.2, and from 1548 to 1833 Ma, respectively (Fig. 6; Supplementary Table S2).

Daerlong pluton

Two samples from the Daerlong pluton were dated; they are both granodiorites (14GW364, 14GW366). Zircons from the two samples are generally euhedral and prismatic in shape and exhibit fine-scale oscillatory zoning (Fig. 4). Twenty-five spots were analyzed on 25 zircons from sample 14GW364. Excluding 13 spots with discordant ages, the remaining 12 analyses define a weighted mean age of 275 ± 2 (MSWD = 0.78, Fig. 5i). Twenty-five zircons from sample 14GW366 were analyzed and the $^{206}Pb/^{238}U$ ages obtained range from 266 to 503 Ma, yielding one group of concordia ages: 274 ± 2 Ma (MSWD = 1.50, n = 15), and ten older inherited grains of ages: ~295 Ma (n = 2), ~315 Ma (n = 4), 382 and 503 Ma (Fig. 5j). The crystallization ages of the two samples are the same within errors, indicating that the Daerlong pluton was emplaced in the Early Permian (~275 Ma). Twenty of the dated zircons of sample 14GW366 were conducted for Lu–Hf isotopes, and 11 data with ages of ~275 Ma have initial $^{176}Hf/^{177}Hf$ ratios of 0.281987–0.282355, with $\varepsilon_{Hf}(t)$ and T_{DM2} values varying from −7.6 to −1.3, and from 1376 to 1774 Ma, respectively (Fig. 6; Supplementary Table S2).

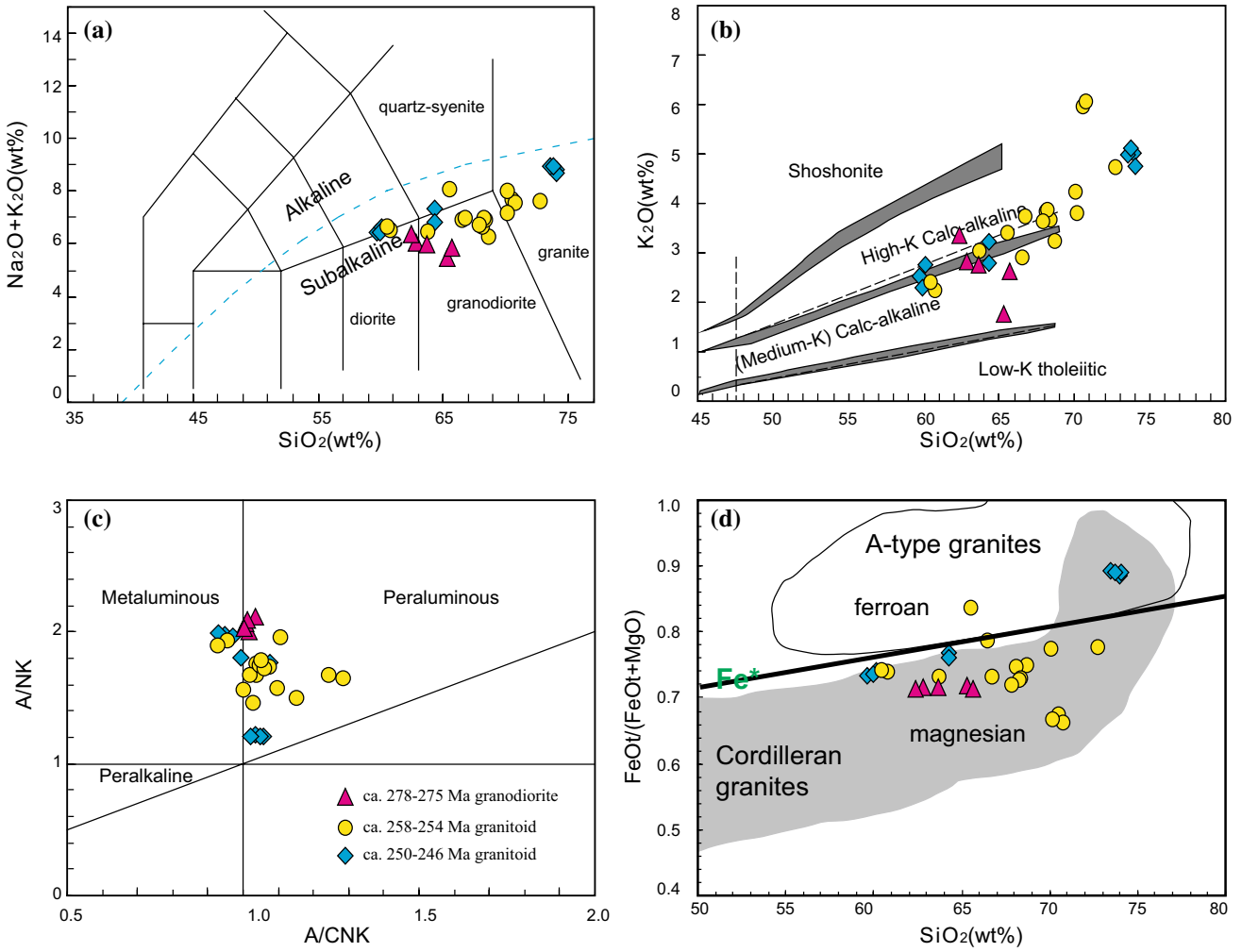

Fig. 7 **a** Total alkali versus SiO_2 classification (TAS, after Irvine and Baragar 1971), **b** K_2O versus SiO_2 classification, after Peccerillo and Taylor (1976), **c** A/NK versus A/CNK classification, after Maniar and Piccoli (1989) and **d** FeOt/(FeOt + MgO) versus SiO_2 diagram, after Frost et al. (2001), Fe* = FeOt/(FeOt + MgO)

Whole-rock geochemistry

The major and trace element compositions of the Early Permian, Late Permian, and Early Triassic granitoid samples are given in Supplementary Table S3.

Early Permian granodiorite

The Early Permian granodiorites of the Daerlong pluton have SiO_2 = 62.38–65.67 wt%, TiO_2 = 0.66–1.03 wt%, total Fe_2O_3 = 4.54–5.50 wt%, MgO = 1.59–1.95 wt%, Al_2O_3 = 15.84–16.93 wt%, and Na_2O/K_2O = 0.85–1.95 (Supplementary Table S3). They are classified in the subalkalic series on a plot of total alkalis against SiO_2 (TAS; Fig. 7a; Irvine and Baragar 1971) and assigned to the medium-K to high-K calc-alkaline igneous rocks on the K_2O versus SiO_2 diagram (Fig. 7b; Peccerillo and Taylor 1976). Their A/CNK [molar $Al_2O_3/(CaO + K_2O + Na_2O)$] values range from 1.00 to 1.04, indicative of weakly peraluminous granites (Fig. 7c; Maniar and Piccoli 1989). Relatively low Fe* [Fe* = FeOt/(FeOt + MgO)] values of 0.71–0.72 classify them as magnesian granitoids (Fig. 7d; Frost et al. 2001). On the FeOt/(FeOt + MgO) versus SiO_2 diagram (Fig. 7d; Frost et al. 2001), they plot in the field of Cordilleran granites which are considered as I-type granites of Chappell and White (1974) and equivalent to the volcanic arc granites of Pearce et al. (1984) or island arc and continental arc granitoids of Maniar and Piccoli (1989). In the chondrite-normalized REE diagram (Fig. 8a), they are characterized by slightly LREE enrichment patterns with $(La/Yb)_N$ values of 5.13–18.2. Except for sample 14GW364 (δEu = 0.97), the remaining samples show obviously negative Eu anomalies (δEu = 0.41–0.74). In the primitive-mantle-normalized trace element diagrams (Fig. 8b), they show

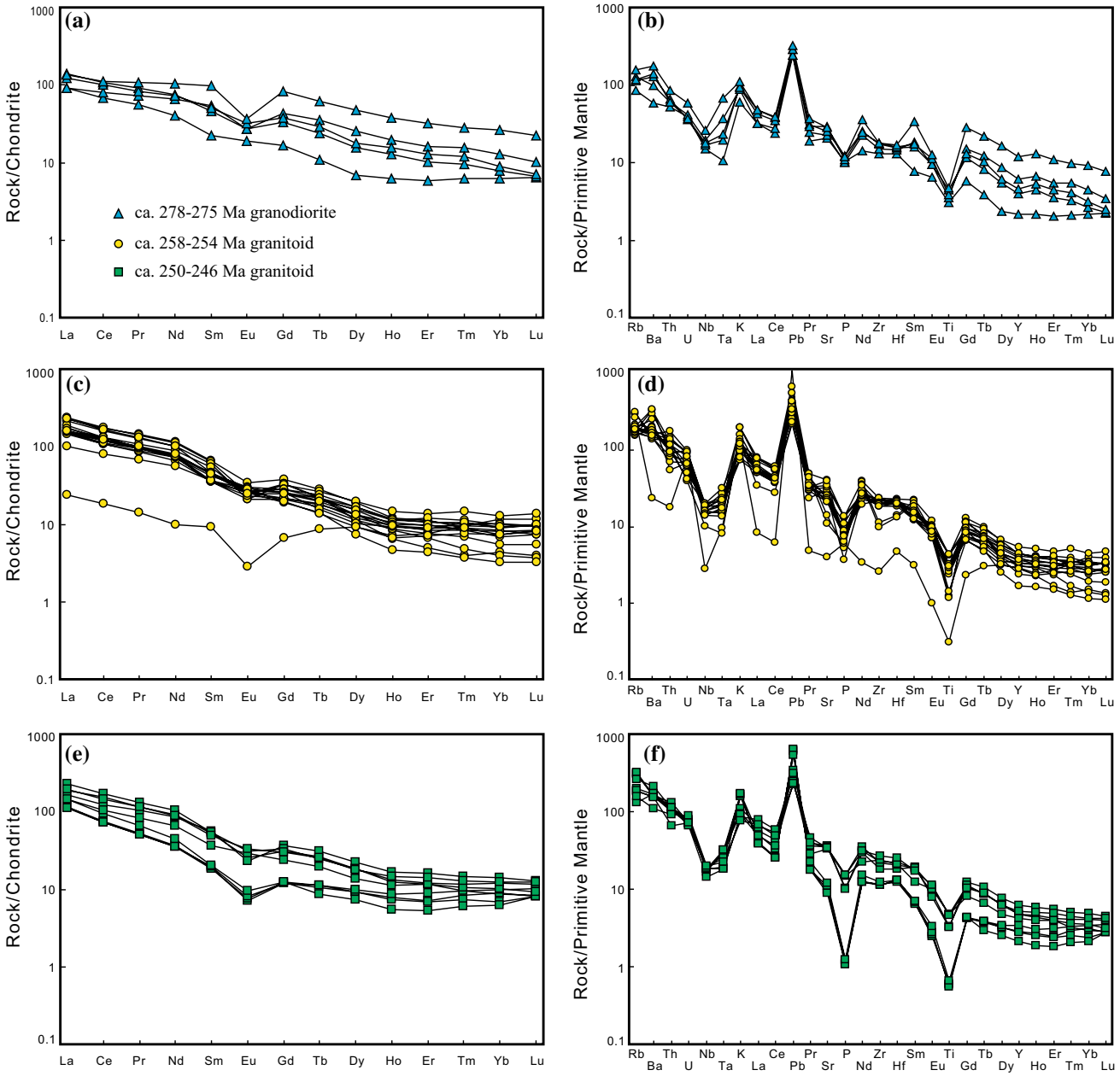

Fig. 8 Chondrite–normalized REE patterns (**a**, **c**, **e**) and primitive-mantle (PM)-normalized trace element (**b**, **d**, **f**) diagrams for the Permian–Early Triassic granitoids from the Gucheng-Boli region. The values of chondrite and PM are from Sun and McDonough (1989)

similar patterns, although there are notable differences in the absolute element concentrations (Supplementary Table S3). All samples are enriched in Rb, Ba, Th, K, Pb, and LREEs, but are depleted in HREEs, Nb, Ta, and Ti with no obvious anomalies of Zr, Hf, and Sr (Fig. 8b).

Late Permian granitoid

The 258–254 Ma granitoids are represented by granodiorites, monzogranites and syenogranites from the Fuxing, Jinfeng, Shengchan II, Dongfanghong and Damadang plutons. They exhibit relatively variable major element compositions, with SiO_2 = 60.49–72.77 wt%, MgO = 0.41–1.90 wt%, Mg# values = 29.1–51.6, and Na_2O/K_2O = 0.22–1.84 (Supplementary Table S3). They belong to high-K to shoshonitic calc-alkaline series (Fig. 7b) and show partly peraluminous features with ACNK ratios of 0.93–1.29 (Fig. 7c). On the FeOt/(FeOt + MgO) versus SiO_2 diagram (Fig. 7d), most granitoid samples occupy the field of magnesian Cordilleran granites. In addition to

sample 14GW070 exhibiting a relatively flat REE pattern with a negative Eu anomaly (Fig. 8c), the other samples show LREE enrichments ($(La/Yb)_N$ = 12.4–54.0) with slightly negative or no obvious Eu anomalies (δEu = 0.47–1.06). These samples contain variable Sr (85–866 ppm) and Y (8–24 ppm) contents with relatively low Sr/Y ratios (6–71, with average of 34). All the samples exhibit enrichments in Rb, Th, U, K, Pb, and LREEs, and depletions in HREEs, Nb, Ta, and Ti with no obvious anomalies of Zr, Hf, and variable Sr and Ba anomalies (Fig. 8d).

Early Triassic granitoid

The 250–246 Ma granitoids consist of quartz diorites, granodiorites and syenogranites from the Tuchengzi, Shengchan I and Hexing plutons. These samples display the following geochemical characteristics: (1) variable SiO_2 content of 59.67–74.04 wt% and low to medium Mg# (20.1–43.2) with medium to high Na_2O/K_2O ratios of 0.71–1.70; (2) high-K calc-alkaline series with ACNK ratios of 0.93–1.07, classifying them as metaluminous to weakly peraluminous granitoids (Fig. 7b, c); (3) relatively high Fe* values of 0.73–0.89, indicative of a ferroan to magnesian feature (Fig. 7d); (4) fractionated REE patterns with $(La/Yb)_N$ values of 11.3–23.7 and weakly negative Eu anomalies (δEu = 0.46–0.98) (Fig. 8e); and (5) low concentrations of Cr and Ni and low ratios of Sr/Y with negative Nb, Ta, Ti and P anomalies, but positive Rb and K anomalies, and no obvious Th, U, Zr, Hf, Sr and Ba anomalies (Fig. 8f).

Discussion

Permian–Early Triassic (ca. 275–245 Ma) continental arc magmatism in the WJB

Zircon U–Pb dating results of the granitoids from the Daerlong, Damadang, Dongfanghong, Shengchan II, Jinfeng, Fuxing, Tuchengzi, Hexing and Shengchan I plutons show that they were emplaced in the Gucheng-Boli region during a short time period between 278 ± 3 and 246 ± 2 Ma. Prior to this study, some intrusive rocks with approximately indistinguishable ages have been recognized in other parts of the WJB (Table 2), including the ~270 Ma Qingshan, ~267 Ma Shichang, ~256 Ma Chushan and ~254 Ma Chaihe granodiorites and monzogranites in the northern Mudanjiang (Wu et al. 2001), the ~265 Ma Yongqing granodiorites in the western Shuangyashan (Zhang et al. 2013), the ~259 Ma Meizuo granodiorites in southern Huanan (Huang et al. 2008), the ~256 Ma Taipinggou gabbros in the northern Luobei (Li et al. 2010; our unpublished data), and the ~272 to 250 Ma Pingdingshan monzogranites in southeastern Jiayin (Bao et al. 2014). These ages indicate that extensive Permian to Early Triassic magmatism occurred continuously at least from ca. 275 to 245 Ma over more than 400 km in extent in the WJB (Fig. 2a).

As shown above, the granitoids studied in this paper as well as the coeval intrusive rocks within the WJB are characterized by variable SiO_2 contents and a rock association of granodiorite, monzogranite, syenogranite, quartz diorite and minor gabbro, similar to those of the continental arc magmatism (e.g. Wilson 1989) as is also revealed by their calc-alkalic compositions, the LREEs and LILEs enrichments and negative Nb, Ta and Ti anomalies (Fig. 8), which are characteristic features shared by many subduction-related magmatic rocks (e.g. Rogers and Hawkesworth 1989; Murphy 2007). Formation of the Permian–Early Triassic granitic rocks in continental arc setting is further confirmed by the different trace element discrimination diagrams (Fig. 9), of which almost all the samples fall into the volcanic arc granite field (VAG), pre-collisional granite field and normal continental arc field in the plots of Nb versus Y (Fig. 9a), Rb versus Nb + Y (Fig. 9b), R_2 versus R_1 (Fig. 9c) and Rb/Zr versus Nb (Fig. 9d), respectively. Furthermore, their N–S-trending linear distributions (Fig. 2a) are very similar to the present-day circum-Pacific magmatic arc (Jahn 1974; Cawood et al. 2009). Therefore, the voluminous intrusive rocks with ages of ca. 275–245 Ma are interpreted to constitute fragments of a magmatic continental arc with an N–S orientation in the WJB.

Petrogenesis

Early Permian granodiorite

The Early Permian granodiorite samples of the Daerlong pluton display similar geochemical compositions (Figs. 7, 10; Supplementary Table S3). They have intermediate SiO_2 contents (62.38–65.67 wt%) and high Na_2O/K_2O ratios (0.85–1.95) with moderate Mg# values (44.9–45.8) and low Cr and Ni concentrations, indicating a crustal source. Although the Mg# values of these granodiorites (44.9–45.8) are slightly higher than those of experimental melts from infracrustal rocks (usually with Mg# values lower than 43; Patiño Douce 1995; Patiño Douce and Beard 1995), the significant injection of mantle-derived magma can be precluded as evidenced by the uniform geochemical and zircon Hf isotopic compositions as well as the general absence of MMEs (Table 1). In the petrogenetic diagram of AFM versus CFM (Fig. 11a), these granodiorite samples plot in the field of partial melts from metabasaltic to metatonalitic sources (Altherr et al. 2000). Moreover, a low and restricted range of Rb/Ba, Rb/Sr, and $Al_2O_3/(FeOt + MgO + TiO_2)$ ratios and a relatively wide range in total contents of $Al_2O_3 + FeOt + MgO + TiO_2$ (Fig. 11b, c) strongly suggest that the crustal source

Table 2 Petrological features and radiometric ages of the Permian to Earliest Triassic arc-type igneous rocks along the eastern NE China

No.	Sample no.	Sample location	Lithology	Igneous classification	Method	Age (Ma)	References
Western margin of the Jiamusi Block							
1	PDS5-1	Pingdingshan	Monzogranite	I-type granite	LA-ICP-MS	272 ± 2	Bao et al. (2014)
2	PDS7-1	Pingdingshan	Monzogranite	I-type granite	LA-ICP-MS	250 ± 3	Bao et al. (2014)
3	07LB16	Taipinggou	Metagabbro		LA-ICP-MS	256 ± 1	Li et al. (2010)
4	12YQ01	Yongqing	Granodiorite	I-type granite	LA-ICP-MS	265 ± 1	Zhang et al. (2013)
5	MZ06	Meizuo	Granodiorite	I-type granite	LA-ICP-MS	259 ± 4	Huang et al. (2008)
6	98SW119	Qingshan	Gneissic granodiorite	I-type granite	SHRIMP	270 ± 4	Wu et al. (2001)
7	M9B	Shichang	Gneissic granodiorite	I-type granite	SHRIMP	267 ± 2	Wu et al. (2001)
8	97SAW028	Chushan	Gneissic granodiorite	I-type granite	SHRIMP	256 ± 5	Wu et al. (2001)
9	97SAW027	Chaihe	Gneissic granodiorite	I-type granite	SHRIMP	254 ± 4	Wu et al. (2001)
10	14GW073	Shengchan I	Granodiorite	I-type granite	LA-ICP-MS	249 ± 4	This study
11	14GW079	Hexing	Syenogranite	I-type granite	LA-ICP-MS	246 ± 2	This study
12	14GW088	Tuchengzi	Quartz diorite	I-type granite	LA-ICP-MS	250 ± 2	This study
13	14GW067	Fuxing	Granodiorite	I-type granite	LA-ICP-MS	256 ± 2	This study
14	14GW068	Jinfeng	Syenogranite	I-type granite	LA-ICP-MS	254 ± 2	This study
15	14GW074	Shengchan II	Monzogranite	I-type granite	LA-ICP-MS	258 ± 2	This study
16	14GW083	Dongfanghong	Granodiorite	I-type granite	LA-ICP-MS	253 ± 3	This study
17	14GW107	Damadang	Granodiorite	I-type granite	LA-ICP-MS	258 ± 2	This study
18	14GW364	Daerlong	Granodiorite	I-type granite	LA-ICP-MS	275 ± 2	This study
19	14GW366	Daerlong	Granodiorite	I-type granite	LA-ICP-MS	274 ± 2	This study
Eastern margin of the Songliao Block							
20	P6-3	Sihaolinchang	Monzogranite	I-type granite	LA-ICP-MS	261 ± 1	Wei (2012)
21	P10-2	Sihaolinchang	Granodiorite	I-type granite	LA-ICP-MS	244 ± 2	Wei (2012)
22	1009-1	Dafeng	Monzogranite	I-type granite	LA-ICP-MS	261 ± 1	Wei (2012)
23	1006-1	Dalazi	Monzogranite	I-type granite	LA-ICP-MS	262 ± 2	Wei (2012)
24	1007-1	Fenglinlinchang	Monzogranite	I-type granite	LA-ICP-MS	264 ± 1	Wei (2012)
25	P18-9	Sandaolinchang	Gneissic monzogranite	I-type granite	LA-ICP-MS	260 ± 1	Wei (2012)
26	HB-1	Yuquan	Rhyolite		LA-ICP-MS	294 ± 3	Meng et al. (2011)
27	HB14-1	Yuquan	Basaltic andesite		LA-ICP-MS	293 ± 2	Meng et al. (2011)
28	HB17-1	Fanshentun	Basaltic andesite		LA-ICP-MS	293 ± 2	Meng et al. (2011)
29	HMD4-1	Weihu Mountain	Dacite		LA-ICP-MS	286 ± 2	Meng et al. (2011)
30	HYS1-1	Taiantun	Rhyolite		LA-ICP-MS	291 ± 4	Meng et al. (2011)
31	HYS2-1	Taiantun	Rhyolite		LA-ICP-MS	291 ± 3	Meng et al. (2011)
32	11HNA1	Huangqigou	Quartz diorite	I-type granite	LA-ICP-MS	256 ± 1	Yu et al. (2013a, b)
33	11HNA4	Xiaobeihu	Monzogranite	I-type granite	LA-ICP-MS	255 ± 2	Yu et al. (2013a, b)
34	11HNA11	Lalagou	Granodiorite	I-type granite	LA-ICP-MS	252 ± 2	Yu et al. (2013a, b)
35	DY0519-1	Weicaohe	Monzogranite	I-type granite	LA-ICP-MS	266 ± 1	Wu et al. (2011)
Eastern margin of the Jiamusi Block							
36	10GW240	Liulian	Granodiorite	I-type granite	LA-ICP-MS	284 ± 2	Yu et al. (2013a)
37	11GW070	Liulian	Hornblende gabbro		LA-ICP-MS	278 ± 2	Yu et al. (2013a)
38	11GW041	Renyi	Monzogranite	I-type granite	LA-ICP-MS	261 ± 3	Bi et al. (2014b)
39	13GW197	Renyi	Monzogranite	I-type granite	LA-ICP-MS	278 ± 3	Bi et al. (2014b)
40	10GW251	Jinshan	Granodiorite	I-type granite	LA-ICP-MS	260 ± 8	Bi et al. (2014b)
41	12GW032	Huangfengshan	Monzogranite	I-type granite	LA-ICP-MS	295 ± 3	Yang et al. (2015a)
42	12GW029	Tiexi	Diorite		LA-ICP-MS	296 ± 2	Yang et al. (2015a)
43	12GW010	Chaoxiantun	Monzogranite	I-type granite	LA-ICP-MS	287 ± 3	Yang et al. (2015a)
44	12GW022	Shuangyehu	Granite porphyry	I-type granite	LA-ICP-MS	258 ± 2	Yang et al. (2015a)
45	12GW041	Yangtianzhai	Granodiorite	I-type granite	LA-ICP-MS	257 ± 3	Yang et al. (2015a)

Table 2 continued

No.	Sample no.	Sample location	Lithology	Igneous classification	Method	Age (Ma)	References
46	12GW047	Majiajie	Granodiorite	I-type granite	LA-ICP-MS	262 ± 3	Yang et al. (2015a)
47	HBQ1-1	Quannong	Rhyolite		LA-ICP-MS	291 ± 2	Meng et al. (2008)
48	HBQ3-1	Wujiuqi	Dacite		LA-ICP-MS	286 ± 3	Meng et al. (2008)
49	HBQ18-2	Wujiuqi	Basaltic andesite		LA-ICP-MS	293 ± 2	Meng et al. (2008)
50	HBQ12	Longtou	Rhyolitic tuff		LA-ICP-MS	263 ± 2	Meng et al. (2008)
51	HBQ13	Longtou	Dacite		LA-ICP-MS	263 ± 5	Meng et al. (2008)
52	HBQ14	Lizhongxinan	Dacite		LA-ICP-MS	288 ± 2	Meng et al. (2008)
53	HM4-1	Dongfa	Rhyolite		LA-ICP-MS	264 ± 7	Meng et al. (2008)
54	HM6	Peide	Rhyolite		LA-ICP-MS	268 ± 2	Meng et al. (2008)
55	13HHL-3	Shuguang	Gabbro		LA-ICP-MS	274 ± 2	Bi et al. (2015)
56	13GW044	Shuguang	Plagiogranite		LA-ICP-MS	277 ± 2	Bi et al. (2015)
57	10GW261	Rizhao	Gabbro		LA-ICP-MS	290 ± 3	Bi et al. (2015)
58	11GW096	Rizhao	Hornblende gabbro		LA-ICP-MS	286 ± 2	Bi et al. (2015)
59	11GW097	Rizhao	Hornblende gabbro		LA-ICP-MS	282 ± 2	Bi et al. (2015)
60	RH02-3	Dongfanghong	Hornblende gabbro		SHRIMP	274 ± 4	Sun et al. (2015a)
61	RH02-10	Dongfanghong	Hornblende gabbro		SHRIMP	276 ± 3	Sun et al. (2015a)

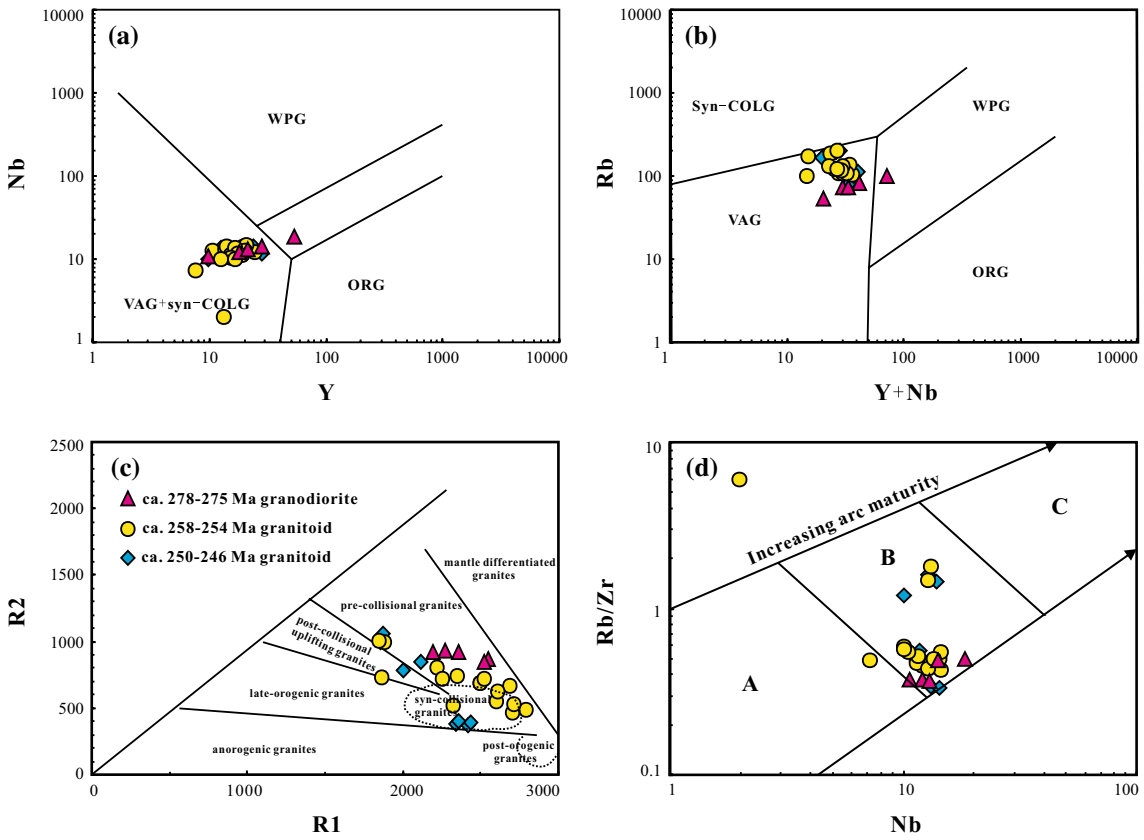

Fig. 9 **a** Nb versus Y diagram, and **b** Rb versus Y + Nb diagram (after Pearce 1996); *ORG* oceanic ridge granites, *post-COLG* post-collisional granites, *syn-COLG* syn-collisional granites, *VAG* volcanic arc granites, *WPG* within-plate granites, **c** R_1 versus R_2 diagram (after Batchelor and Bowden 1985), **d** Nb–Rb/Zr bivariate plot with fields after Brown et al. (1984), *A* primitive island arcs and continental arcs, *B* normal continental arcs and *C* mature continental arcs

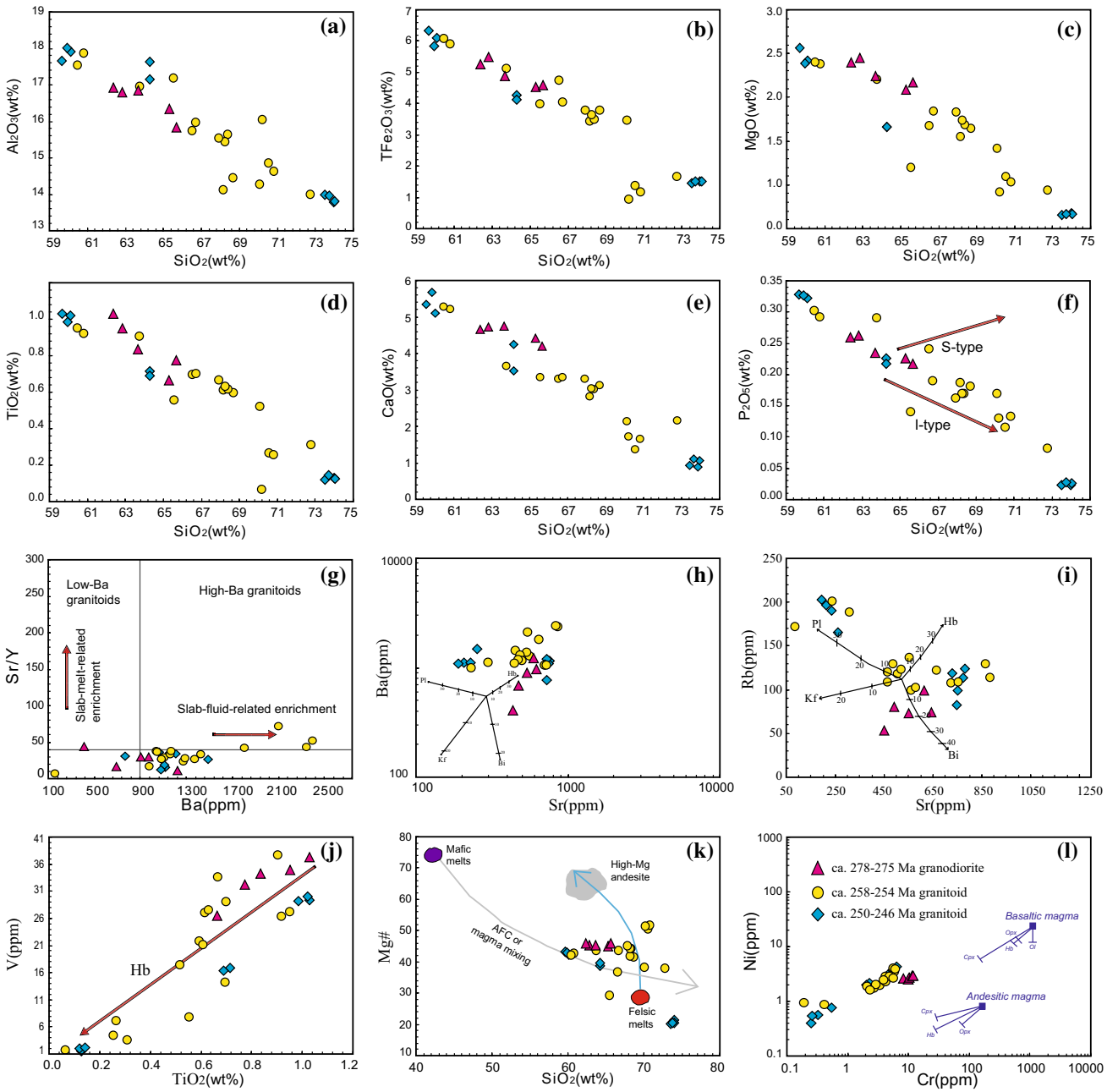

Fig. 10 Major and trace element Harker variation diagrams showing the magmatic evolution of the Middle-Late Triassic granitoids from the Gucheng–Chabaqi region

materials are dominantly composed of basic igneous rocks such as basalts or amphibolites for the Daerlong granodiorite (Sylvester 1998; Patiño Douce 1999). Notably, several experimental studies have shown that dehydration melting of an amphibolite source is likely to generate a low-K tonalitic–trondhjemitic melt rather than a high-K calc-alkaline melt (e.g. Roberts and Clemens 1993; Wyllie et al. 1996). Thus, we favor the illustration proposed by Patiño Douce (1999) that some assimilation of metasediment components by basaltic sources may have occurred at relatively low-pressure conditions to engender high-K abundances in the Daerlong granodiorites (Fig. 7b), as indicated by the frequent occurrence of 295–503 Ma inherited zircon grains (Fig. 5j), and no HREE depletion (Fig. 8a) with low Sr/Y values but high Y concentrations (Fig. 11d). Alternatively, the Daerlong granodiorites have a relatively tight range of $\varepsilon_{Hf}(t)$ values (−7.6 to −1.3) and T_{DM2} ages (1.38–1.78 Ga); therefore, we conclude that the Early Permian granodioritic magma was derived chiefly from the partial melting of pre-existing ancient basaltic materials in lower crust with

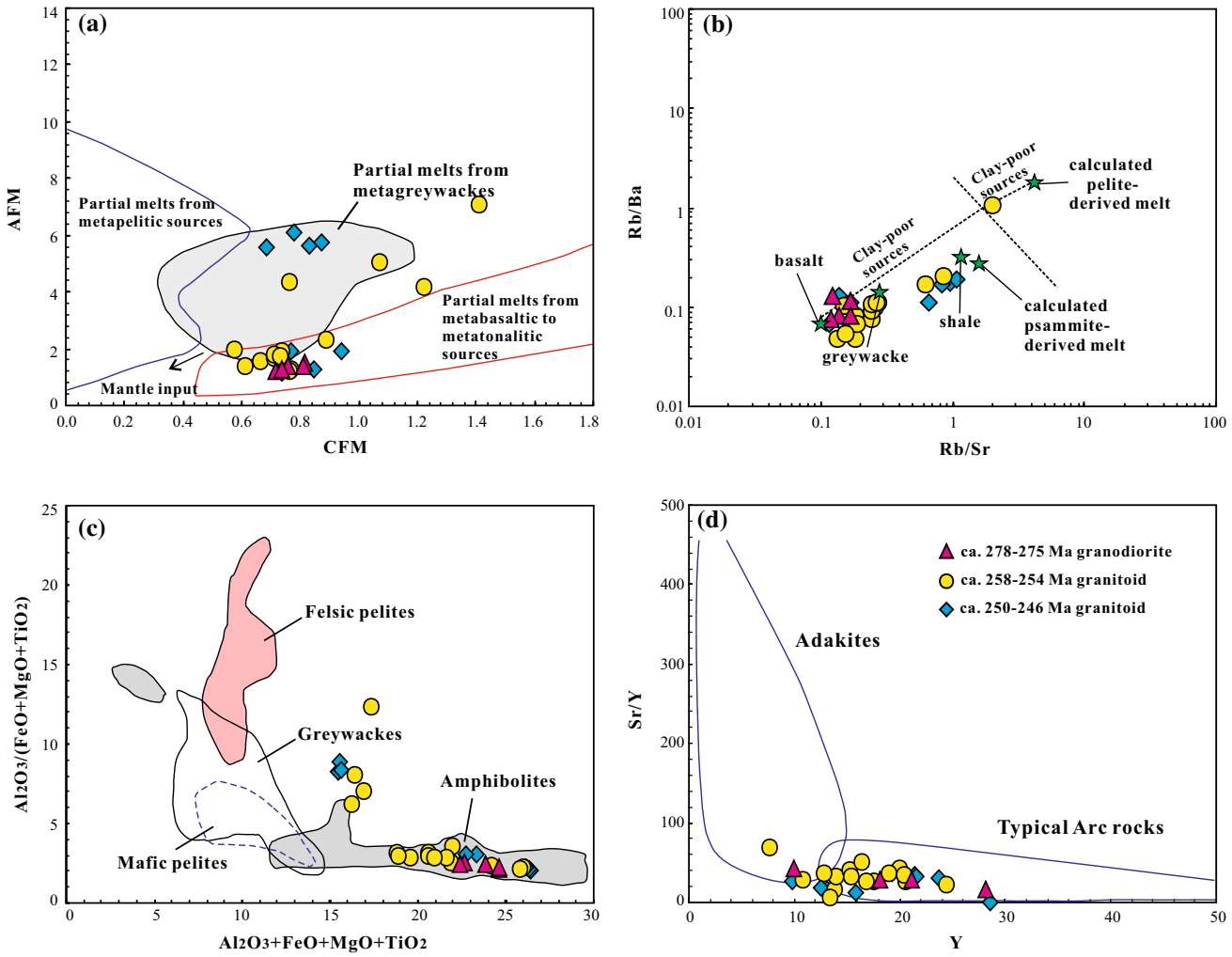

Fig. 11 **a** Molar $Al_2O_3/(FeOT + MgO)$ (AFM) versus molar $CaO/(FeOT + MgO)$ (CFM) diagram, revised after Altherr et al. (2000), **b** Rb/Ba versus Rb/Sr diagram, fields and trends are after Sylvester (1998), **c** $Al_2O_3/(FeO + MgO + TiO_2)$ versus $Al_2O_3 + FeO + MgO + TiO_2$ diagram, fields and trends are after Patiño Douce (1999) and **d** Sr/Y versus Y diagram (after Defant and Drummond 1990)

involvement of assimilation of metasediment components under low pressures during magma ascent. This conclusion is further supported by Shellnutt and Dostal (2015), who have conducted the equilibrium partial melt modeling using program MELTS and found the best result that produced the granodiorites was from a mixed meta-sedimentary and meta-basaltic source with an initial water content of 1.0 wt% and a fO_2 value of FMQ + 1.

Late Permian and Early Triassic granitoids

As described earlier, the Late Permian (258–254 Ma) rocks consist of a suite of granodiorites, monzogranites and syenogranites, while the Early Triassic (250–246 Ma) rocks are represented by a quartz diorite–granodiorite–syenogranite association. Although these units do not coexist within plutons, they have similar geochemical variations and zircon Hf isotopic compositions (Fig. 10; Supplementary Table S2, S3), indicating a common source or petrogenetic process. Both the two stages of granitoids have a wide range of SiO_2 (59.67–74.04 wt%) and MgO contents (0.16–2.06 wt%), and high Y concentrations with low Sr/Y values, similar to igneous rocks in modern arcs (Fig. 11d). Furthermore, the granitoid samples show variable LREE enrichment patterns with weak negative or no obvious Eu anomalies ($\delta Eu = 0.46–1.06$) (Fig. 8c, e), implying that their source region was composed dominantly of plagioclase and hornblende without garnet (Patiño Douce and Beard 1995; Rapp and Watson 1995). The petrogenetic diagrams of AFM versus CFM (Fig. 12a), Rb/Ba versus Rb/Sr (Fig. 11b), and $Al_2O_3/(FeOt + MgO + TiO_2)$ versus $Al_2O_3 + FeOt + MgO + TiO_2$ (Fig. 11c) indicate that the

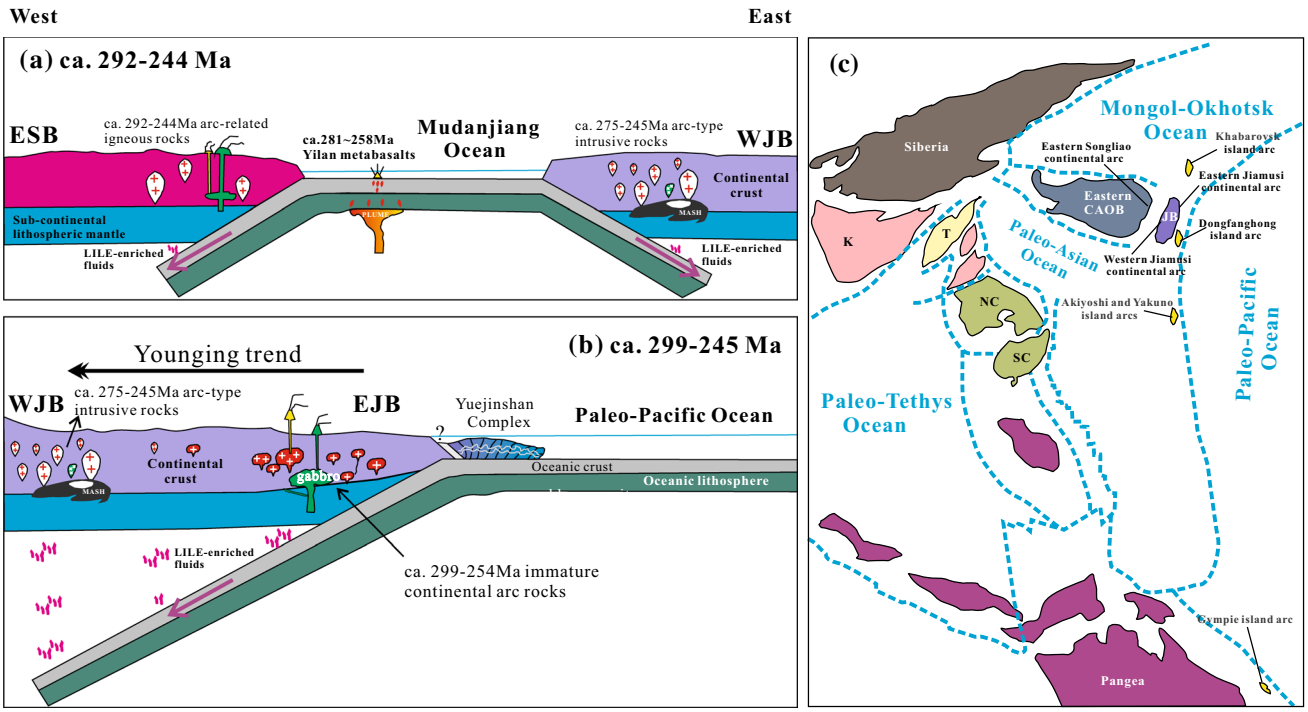

Fig. 12 **a**, **b** Schematic diagram showing two possible tectonic models for the Permian–Early Triassic granitoids from the WJB, see the text for detailed explanation and **c** modified Permian global plate reconstruction map showing the locations of the Paleo-Pacific Khabarovsk, Dongfanghong, Jiamusi, Akiyoshi, Yakuno, and Gympie areas (after Zhang 1997; Sun et al. 2015a and references cited therein). *K* Kazakhstan, *T* Tarim Craton, *NC* North China Craton, *SC* South China Craton, *JB* Jiamusi Block

Late Permian–Early Triassic granitic melts were derived from miscellaneous crustal materials chiefly composed of igneous rocks (e.g. basalt and its equivalents) and partially clay-poor sedimentary rocks including graywackes and shales (Sylvester 1998; Patiño Douce 1999; Altherr et al. 2000). In the Mg# versus SiO_2 diagram (Fig. 10k), it is evident that the 258–246 Ma granitoid samples show a trend defining an AFC or magma mixing process, distinct from that of felsic melt-peridotite interaction on the basis of experimental results (Rapp et al. 1999). The evident systematic trends between SiO_2 and other major and trace elements indicate that crystal fractionation occurred during magma evolution (Fig. 10). Clinopyroxene (Cpx) and hornblende (Hb) are potential fractional phases that account for the decreases in MgO, TFe_2O_3, and CaO with increasing SiO_2 (Fig. 10b, c, e), which is further supported by the covariations between Sr and Ba, TiO_2 and V as well as Ni versus Cr (Fig. 10h, j, l). The Al_2O_3 decreases with increasing SiO_2 and covariations between Sr and Rb and Ba (Fig. 10a, i) suggest plagioclase (Pl) is a major fractionated phase. Likewise, separation of accessory minerals such as apatite (Ap) and Fe–Ti oxides could explain the observed reductions in P_2O_5 and TiO_2 with increasing SiO_2 (Fig. 10d, f), and depletions in P and Ti (Fig. 8d, f).

A fractional mineral assemblage of (Cpx + Hb + Pl + Ap + Fe–Ti oxides) could explain the systematic elements variations observed in the 258–246 Ma granitoid samples. However, no single closed-system fractionation processes can produce the variable isotopic compositions in these samples ($\varepsilon_{Hf}(t) = -22.9$ to $+1.7$; Fig. 6). This finding indicates that wall-rock assimilation or magma mixing may potentially explain these isotopic features. Firstly, four of the eight dated samples contain inherited zircons with ages of 275–734 Ma (Fig. 5d, e, g, h), together with the observations that most plutons intruded the Mashan supracrustal rocks (Fig. 3a), indicating some crustal assimilation did take place during magma evolution. Secondly, it is commonly found that zircons having homogeneous U–Pb ages but with variable Hf isotopic compositions are the result of magma mixing of magmas derived from distinct source rocks (e.g. Belousova et al. 2006; Yang et al. 2008). Notably, some of the measured zircon grains have $\varepsilon_{Hf}(t)$ values varying from +0.2 to +1.6, demonstrating that some depleted mantle components with high positive $\varepsilon_{Hf}(t)$ values have been involved in the melting source. This conclusion is also supported by the common occurrences of mantle-derived MMEs (Fig. 3b, d, e) and relatively high Mg# values (43.6–51.2, average of 46.7) of the

Fuxing, Jinfeng and Damadang plutons. In summary, the Late Permian and Early Triassic granitoids might be generated from the miscellaneous crustal materials composed of dominantly igneous rocks and partially clay-poor sedimentary rocks, coupled with involvement of depleted mantle-derived melts, assimilation with crustal wall-rocks, and fractional crystallization during magma generation, ascent and emplacement.

Implications for the MASH hypothesis

Our data discussed above reveal that materials from multi-sources, multi-stages might have been incorporated during the magma genesis of the granitoid rocks from the WJB. Many studies in Andes have demonstrated enriched incompatible trace element compositions in continental arc magmas traversing thick crust as compared to those traversing thin crust (e.g. McMillan et al. 1993). Thus, the LILE and LREE enrichments in the WJB granitoids (Fig. 8) suggest involvement of thick continental crust through which the magma traversed. In addition, as described in Whalen et al. (1999), plot of Ba versus Sr/Y is considered to discriminate between a slab-melt-related and slab-fluid-related enrichment in the mantle wedge. Our granitoid samples generally exhibit low Sr/Y values with significant Ba enrichment trend from 164 to 2400 ppm (Fig. 10g), suggesting that, initially, slab generated fluids probably caused LILE enrichment in the WJB source magma. All these features are consistent with continental arcs in western South and North America, where materials from subducted oceanic slab, mantle wedge and continental crust could be involved and their source areas could be temporally and spatially different (e.g. Feeley et al. 1998; Mamani et al. 2010). Collectively, we infer that melting, fractional crystallization, assimilation, storage, and homogenization (MASH) processes proposed by Hildreth and Moorbath (1988) may have occurred during formation of the studied granitoids (Fig. 12a, b). Firstly, LILE-enriched fluids were generated through dehydration of the upper part of subducting oceanic lithosphere, when interacting with the overlying mantle wedge. Subsequently, these ascending LILE-enriched fluids induced partial melting of the mantle wedge, continuously impelling the rising basaltic melts to pond at the base of thick crust as a MASH zone, where conditions are favorable for high-volume dehydration partial melting of pre-existing ancient lower-crustal rocks to produce fractionated, buoyant, possibly hybrid granitic melts. At last, such granitic melts must have experienced crustal assimilation-fractional crystallization (AFC) processes while ascending through thick crust to their final level of emplacement.

Crustal evolution of the Jiamusi Block and the relationships to the Songliao Block

Granitic rocks are among the most important constituents of the Earth's continental crust and play an important role in deciphering crustal growth through geological times (e.g. Wu et al. 2011). So far, two major periods of granitoids with ages between 540–484 and 299–246 Ma have been identified, which thus can provide important clues to understand the crustal nature and evolution of the Jiamusi Block. Zircon Hf isotopic data show that both the 540–484 and 299–246 Ma granitoids have $\varepsilon_{Hf}(t)$ values overlapping the chondritic uniform reservoir value (Fig. 6a), with the two-stage Hf model ages (i.e., ca. 1.2–2.4 Ga and ca. 1.0–2.8 Ga, respectively) being significantly older than their crystallization ages (Supplementary Table S1, S2). This suggests that reworking of ancient crust mainly occurred during the Early Cambrian, Permian, and Early Triassic. However, some samples, especially those in the eastern margin of the Jiamusi Block (EJB), have relatively high and positive $\varepsilon_{Hf}(t)$ values (e.g. Yu et al. 2013a; Yang et al. 2015a; Fig. 6), indicating significant injection of juvenile materials that were probably derived directly from depleted mantle might also have involved in the crustal source. In addition, it is evident that the $\varepsilon_{Hf}(t)$ values of zircons from the 540–484 and 299–246 Ma granitic rocks are mostly located in the crustal evolution region of the Jiamusi Block as estimated by the isotopic evolved tendency and average two-stage Hf model ages (ca. 1.4–2.1 Ga; Fig. 6a). All the above information suggests that crustal growth in the Jiamusi Block mainly occurred in the Paleo-Mesoproterozoic, whereas reworking of the ancient crust and some accretion of new crust took place in the early Paleozoic and Permian–Early Triassic. Furthermore, it is worthy noting that the 278–246 Ma granitoids in the WJB have distinct zircon Hf isotopic characteristics from those of the nearly coeval granitoids in the EJB, i.e., the $\varepsilon_{Hf}(t)$ values of the granitic rocks decrease from west to east (Fig. 6b), implying the magma sources in the east involved more juvenile components than in the west, and further revealing the heterogeneity of deep crust in the Jiamusi Block.

At present, some researchers proposed that the Jiamusi Block was rifted from the Songliao Block of the CAOB sometime before or around 275–258 Ma (Zhou et al. 2009; Zhu et al. 2015). More recently, Zhu et al. (2016) further argued that the continental rifting between the joint Jiamusi and Songliao blocks took place during Permian to Triassic time and continued its evolution into an open ocean that subsequently closed after ~140 Ma. In this paper, however, our data fail to favor the Jiamusi-Songliao link for the following reasons. Firstly, the crustal basement of the Songliao Block consists mainly of Mesozoic granitoids and

Paleozoic strata with minor Precambrian components (e.g. Wu et al. 2002; Wang et al. 2006; Pei et al. 2007). Systematic zircon Lu–Hf and whole-rock Sr–Nd isotopic studies indicate that the Songliao Block contain a large proportion of juvenile crustal material, and continental growth in this block occurred during the Neoproterozoic to Cambrian (ca. 0.5–2.1 Ga), whereas reworking and accretion of new crust mainly took place during the Permian–Jurassic (e.g. Wu et al. 2000, 2003; Meng et al. 2011; Yu et al. 2013b). As pointed out above, the crustal nature and evolution of the Jiamusi Block is devoid of these events of the Songliao Block. Secondly, the Pre-Permian sedimentary sequences in the easternmost Songliao Block (ESB) have significant differences with those in the WJB (HBGMR 1993; Meng et al. 2011), of which the former contains no Pan-African khondalitic records but has widespread late Paleozoic volcanic-sedimentary rocks. Therefore, a pre-Permian correlation of the Jiamusi Block and the Songliao Block is questionable. Thirdly, geochemical and geochronological data show that the WJB developed in a continental arc setting during in the Permian–Early Triassic (ca. 275–245 Ma), not a continental rift environment as supposed by Zhou et al. (2009) and Zhu et al. (2015, 2016). Taken together, we argue that the Jiamusi Block was unlikely the rifted segment of the Songliao Block.

Possible tectonic evolution models

As outlined earlier, the massive granitoids and minor gabbros with ages of ca. 275–245 Ma constitute an N–S-trending arc magmatic belt in the WJB, nearly parallel to the distribution of the Heilongjiang Complex (Fig. 2a). In addition, the coeval 292–244 Ma mafic to felsic igneous rocks with arc-affinity (mostly I-type granitoids and their eruptive counterparts, Meng et al. 2011; Wu et al. 2011; Wei 2012; Yu et al. 2013b; our unpublished data) in the Lesser Xing'an and Zhangguangcai ranges also distribute around the Heilongjiang Complex in a north–south direction (Fig. 2a). The Heilongjiang Complex between the Jiamusi and Songliao blocks is the remains of a paleo-ocean named Mudanjiang Ocean by Wu et al. (2011), records complex subduction, collision and accretion processes and therefore probably becomes the key to interpret the formation of these N–S-trending arc magmatic belts. As significant components of the Heilongjiang complex, the blueschists are well exposed along the Mudanjiang Fault, geochronological data show that they partly formed during the Permian with protolith ages between 281 ± 3 and 258 ± 2 Ma (Zhou et al. 2009; Ge et al. 2015; Zhu et al. 2015). Moreover, the geochemical characteristics indicate that the protoliths of the blueschists have OIB affinities (Zhou et al. 2009; Ge et al. 2015; Zhu et al. 2015), together with the unlikely linkage between the Jiamusi and Songliao blocks, we infer that they may be generated in an ocean island setting, in other words, the Mudanjiang Ocean existed at least since the Early Permian, and its subduction may have initiated at that time (Ge et al. 2015). In particular, most of lithologies in the eastern NE China were only metamorphosed in sub-greenschist to greenschist facies (e.g. HBGMR 1993; Zhou et al. 2009; Zhu et al. 2016), unlike other typical continent–continent collisional belts resulted from a single-sided subduction that contain large amounts of high-grade metamorphic rocks forming at the subduction stage of continental crust following the closure of an ancient ocean (Zhao 2015). To summarize the above discussion, we proposed a possible divergent double-sided subduction model for the formation and evolution of the eastern NE China (Fig. 12a). In the period 292–244 Ma, the Jiamusi and Songliao blocks were separated by the Mudanjiang Ocean whose lithosphere was undergoing divergent double-sided subduction beneath the eastern margin of the Songliao Block (ESB) and the western margin of the Jiamusi Block (WJB). This type of double subduction evolution involved the development of magmatic arcs on both the active continental margins (Fig. 2a), represented by the ca. 292–244 Ma Fengmao, Shangzhi, and Xiaobeihu arc-type igneous rocks at the ESB and the ca. 275–245 Ma Luobei, Linkou and Mudanjiang arc-related intrusive rocks on the WJB.

The above divergent double-sided subduction model is based on the assumption that the WJB has been located in the vicinity of the Songliao Block and influenced by the tectonic evolution of the Mudanjiang Ocean since the Early Permian. An increasing number of data have been reported that favor an exotic origin, possibly Gondwana, for the Jiamusi Block (e.g. Wilde et al. 1999, 2000; Wu et al. 2011; Yang et al. 2014, 2015a); therefore, an alternative interpretation that the Jiamusi Block is a drifting terrane situated in an area slightly far from the Songliao Block during the Permian and the ca. 275–245 Ma granitoids of the WJB were emplaced in a continental arc setting related to westward subduction of the Paleo-Pacific Ocean is also possible (Fig. 12b). This model is supported by the recent studies by Yu et al. (2013a), Yang et al. (2015a, b) and Sun et al. (2015a), in which the spatial configuration of the ca. 299–254 Ma immature continental arc rocks in the eastern margin of the Jiamusi Block (EJB) and the ~275 Ma immature island arc Dongfanghong gabbro in the Yuejinshan Complex to the east is best explained by processes associated with westward subduction of the Paleo-Pacific Plate.

In summary, in the absence of reliable paleo-magnetic and geophysical data, we cannot reach an irrefutable conclusion about which of the two models was responsible for the generation of the studied granitoids in this paper. Nevertheless, it should be noted that some studies (e.g. Zhou et al. 2009; Ge et al. 2015) recently argued that the

Mudanjiang Ocean between Jiamusi and Songliao blocks must be different from the Paleo-Asian Ocean, and in a sense, might also be a part of the Paleo-Pacific Ocean (see details in Ge et al. 2015). Moreover, from a global perspective (Fig. 12c), Permian arc rocks in the Khabarovsk accretionary complex, Russian Far East (Suzuki et al. 2005); the Akiyoshi accretionary complex and Yakuno Ophiolite, SW Japan (Sano 1992; Isozaki 1997); and the Gympie Group in eastern Australia (Sivell and Waterhouse 1988) are also reported along the Western Paleo-Pacific margin. In this context, we propose that all these N–S-trending arc magmatic belts, including the ca. 275–245 Ma intrusions in the WJB, the ca. 292–244 igneous rocks in the ESB, and the ca. 299–254 Ma igneous rocks in the EJB, might not be caused by Paleo-Asian Ocean subduction, instead, they probably represent the magmatic records of the Permian–Early Triassic subduction of the Paleo-Pacific Oceanic Plate beneath the Jiamusi Block, and even whole eastern NE China.

Conclusions

Based on the above discussion, we draw the following conclusions:

1. Extensive Permian to Early Triassic continental arc magmatism occurred continuously at least from ca. 275 to 245 Ma over more than 400 km in extent in the WJB.
2. Petrogenetic considerations indicate that a MASH-like process may have occurred during formation of the studied granitoids. The 278–275 Ma granodiorites were derived from the pre-existing ancient basaltic materials in lower crust with involvement of metasediment assimilation under low pressures during magma ascent. The 258–246 Ma granitic magma might be generated from the miscellaneous crustal source composed of dominantly igneous rocks and partially clay-poor sediments, coupled with mantle-derived melt hybridization, wall-rock assimilation, and fractional crystallization.
3. Continental growth in the Jiamusi Block occurred during the Paleo-Mesoproterozoic, whereas reworking of the ancient crust and accretion of some new crust occurred in the early Paleozoic and Permian–Early Triassic. The crustal nature and the Pre-Permian sedimentary units of the WJB and is distinct from those of the ESB, implying the Jiamusi Block was unlikely the rifted segment of the Songliao Block.
4. In the eastern NE China, these ca. 299–245 Ma mafic to felsic intrusions and their eruptive counterparts constituted an N–S-trending arc magmatic belt, suggesting that Paleo-Pacific Plate subduction was initiated in the Permian to Early Triassic.

Acknowledgments We are grateful to Jinhui Yang and Yueheng Yang of the Institute of Geology and Geophysics, Chinese Academy of Sciences (Beijing), China, for their advice and assistance during zircon U–Pb dating and Lu–Hf isotope analyses. We thank the Beijing Research Institute of Uranium Geology, China, for assistance in analyses of major and trace elements. We also thank Greg Shellnutt, one anonymous reviewer and Editors Wolf-Christian Dullo and Wenjiao Xiao for their constructive comments that helped to improve the manuscript. This work was financially supported by the National Natural Science Foundation of China (41472050, 41330206) and Project 2016034 supported by Graduate Innovation Fund of Jilin University.

References

Altherr R, Holl A, Hegner E, Langer C, Kreuzer H (2000) High-potassium, calc-alkaline I-type plutonism in the European Variscides: northern Vosges (France) and northern Schwarzwald (Germany). Lithos 50:51–73

Amelin Y, Lee DC, Halliday AN (2000) Early–middle Archaean crustal evolution deduced from Lu–Hf and U–Pb isotopic studies of single zircon grains. Geochim Cosmochim Acta 64:4205–4225

Andersen T (2002) Correction of common lead in U–Pb analyses that do not report ^{204}Pb. Chem Geol 192:59–79

Bao ZY, Wang J, Yang YC, Wang L, Xie ZP, Song Y, Liu JG (2014) U–Pb dating and Hf isotopic composition of ore-hosting granites from the Pingdingshan gold deposit, Heilongjiang Province, and its geological implications. Acta Geol Sinica 88(3):407–420

Batchelor RA, Bowden VP (1985) Petrogenetic interpretation of granitoid rock series using multicationic parameters. Chem Geol 48:43–55

Belousova BA, Griffin WL, O'Reilly SY (2006) Zircon crystal morphology, trace element signatures and Hf isotope composition as a tool for petrogenetic modelling: examples from Eastern Australian granitoids. J Petrol 47:329–353

Bi JH, Ge WC, Yang H, Zhao GC, Yu JJ, Zhang YL, Wang ZH, Tian DX (2014a) Petrogenesis and tectonic implications of early Paleozoic granitic magmatism in the Jiamusi Massif, NE China: geochronological, geochemical and Hf isotopic evidence. J Asian Earth Sci 96:308–331

Bi JH, Ge WC, Zhang YL, Yang H, Wang ZH (2014b) Petrogenesis of Permian Jinshan granitic complex in the eastern Jiamusi Massif and its geological implications. J Earth Sci Environ 36(4):16–31 **(in Chinese with English abstract)**

Bi JH, Ge WC, Yang H, Zhao GC, Xu WL, Wang ZH (2015) Geochronology, geochemistry and zircon Hf isotopes of the Dongfanghong gabbroic complex at the eastern margin of the Jiamusi Massif, NE China: petrogensis and tectonic implications. Lithos 234:27–46

Bouvier A, Vervoort JD, Patchett PJ (2008) The Lu–Hf and Sm–Nd isotopic composition of CHUR: constraints from unequilibrated chondrites and implications for the bulk composition of terrestrial planets. Earth Planet Sci Lett 273:48–57

Brown GC, Thorpe RS, Webb PC (1984) The geochemical characteristics of granitoids in contrasting arcs and comments on magma source. J Geol Soc London 141:413–426

Cao X, Dang ZX, Zhang XZ, Jiang JS, Wang HD (1992) Jiamusi composite terranes. Jilin Publishing House of Science and Technology, Changchun **(in Chinese with English and Russian abstracts)**

Cawood PA, Kröner A, Collins WJ, Kusky TM, Mooney WD, Windley BF (2009) Accretionary orogens through earth history. Geol Soc Lond Spec Publ 318:1–36

Chappell BW, White AJR (1974) Two contrasting granite types. Pac Geol 8:173–174

Cheng RY, Wu FY, Ge WC, Sun DY, Liu XM, Yang JH (2006) Emplacement age of the Raohe Complex in eastern Heilongjiang Province and the tectonic evolution of the eastern part of Northeastern China. Acta Petrologica Sinica 22:353–376 **(in Chinese with English abstract)**

Defant MJ, Drummond MS (1990) Derivation of some modern arc magmas by melting of young subducted lithosphere. Nature 347:662–665

Feeley TC, Dungan MA, Frey FA (1998) Geochemical constraints on the origin of mafic and silicic magmas at Cordon El Guadal, Tatara-San Pedro Complex, central Chile. Contrib Miner Petrol 131:393–411

Frost BR, Barnes CG, Collins WJ, Arculus RJ, Ellis DJ, Frost CD (2001) A geochemical classification for granitic rocks. J Petrol 42:2033–2048

Gao FH, Xu WL, Yang DB, Pei FP, Liu XM, Hu ZC (2007) LA-ICP-MS zircon U–Pb dating from granitoids in southern basement of Songliao basin: constraints on ages of the basin basement. Sci China (D) 50:995–1004

Ge MH, Zhang JJ, Liu K, Ling YY, Wang M, Wang JM (2015) Geochemistry and geochronology of the blueschist in the Heilongjiang Complex and its implications in the late Paleozoic tectonics of eastern NE China. Lithos. doi:10.1016/j.lithos.2015.11.019

Griffin WL, Pearson NJ, Belousova EA, Saeed A (2006) Comment: Hf-isotope heterogeneity in standard zircon 91500. Chem Geol 233(3):358–363

HBGMR (Heilongjiang Bureau of Geology and Mineral Resources) (1993) Regional geology of Heilongjiang Province. Geological Publishing House, Beijing, pp 347–418 **(in Chinese with English abstract)**

Hildreth W, Moorbath S (1988) Crustal contributions to arc magmatism in the Andes of central Chile. Contrib Mineral Petrol 98(4):455–489

Huang YC, Ren DH, Zhang XZ, Xiong XS, Zhang CY, Wang Y, Zhao LL (2008) Zircon U–Pb dating of the Meizuo granite and geological significance in the Huanan Uplift, east Heilongjiang Province. J Jilin Univ (Earth Sci Ed) 38(4):631–638

Irvine TH, Baragar WRA (1971) A guide to the chemical classification of the common volcanic rocks. Can J Earth Sci 8:523–548

Isozaki Y (1997) Contrasting two types of orogens in Permo-Triassic Japan: accretionary versus collisional. Isl Arc 6:2–24

Jahn BM (1974) Mesozoic thermal events in southeast China. Nature 248:480–483

Jiang J (1992) Peak regional metamorphism of the khondalite series of Mashan Group and its evolution. Acta Petrologica Et Mineralogica 11:97–108 **(in Chinese with English abstract)**

Khanchuk AI, Vovna GM, Kiselev VI, Mishkin MA, Lavrik SN (2010) First Results of Zircon LA-ICP-MC U–Pb Dating of the Rocks from the Granulite Complex of Khanka Massif in the Primorye Region. Dokl Earth Sci 434(1):1164–1167

Kovalenko VI, Yarmolyuk VV, Kovach VP, Kotov AB, Kozakov IK, Salnikova EB, Larin AM (2004) Isotope provinces, mechanisms of generation and sources of the continental crust in the Central Asian mobile belt: geological and isotopic evidence. J Asian Earth Sci 23:605–627

Kröner A, Windley BF, Badarch G, Tomurtogoo O, Hegner E, Jahn BM, Gruschka S, Khain EV, Demoux A, Winjgate MTD (2007) Accretionary growth and crust formation in the central Asian Orogenic Belt and comparison with the Arabian-Nubian shield. Geol Soc Am Mem 200:181–209

Kröner A, Kovach V, Belousova E, Hegner E, Armstrong R, Dolgopolova A, Seltmann R, Alexeiev DV, Hoffmann JE, Wong J, Sun M, Cai K, Wang T, Tong Y, Wilde SA, Degtyarev KE, Rytsk EYu (2014) Reassessment of continental growth during the accretionary history of the Central Asian Orogenic Belt. Gondwana Res 25(1):103–125

Lehmann J, Schulmann K, Lexa O, Corsini M, Kröner A, Sripská P, Tomurhuu D, Otgonbator D (2010) Structural constraints on the evolution of the Central Asian Orogenic Belt in SW Mongolia. Am J Sci 310:575–628

Lennon RG, Wilde SA, Yang T (1997) The Mashan Group: a 500 Ma granulite facies terrain within the Jiamusi Massif, Heilongjiang Province, North-eastern China. In: Cox R, Ashwal LD (eds) Proterozoic geology of Madagascar, Proceedings of UNESCO-IUGS-IGCP 348/368 international field workshop, Antananarivo, Madagascar, 1997. Gondwana Research Group, Publication 5:45–46

Li JY (2006) Permian geodynamic setting of Northeast China and adjacent regions: closure of the Pale-Asian Ocean and subduction of the Paleo-Pacific Plate. J Asian Earth Sci 26(3):207–224

Li XP, Kong FM, Zheng QD, Dong X, Yang ZY (2010) Geochronological study on the Heilongjiang complex at Luobei area, Heilongjiang Province. Acta Petrologica Sinica 26(7):2015–2024

Ludwig KR (2003) User's manual for Isoplot 3.0: a geochronological toolkit for Microsoft Excel. Berkeley Geochronol Center Spec Publ 4:1–70

Mamani M, Wörner G, Sempere T (2010) Geochemical variations in igneous rocks of the Central Andean orocline (13°S to 18°S): tracing crustal thickening and magma generation through time and space. Geol Soc Am Bull 122:162–182

Maniar PD, Piccoli PM (1989) Tectonic discrimination of granitoids. Geol Soc Am Bull 101:635–643

McMillan NJ, Davidson JP, Warner G, Harmon RS, Moorbath S, Lopez-Escobar L (1993) Influence of crustal thickening on arc magmatism: Navados de Payachata volcanic region, northern Chile. Geology 21:467–470

Meng E, Xu WL, Pei FP, Yang DB, Ji WQ, Yu Y, Zhang XZ (2008) Chronology of Late Paleozoic volcanism in eastern and southeastern margin of Jiamusi Massif and its tectonic implications. Chin Sci Bull 53:1231–1245

Meng E, Xu WL, Pei FP, Yang DB, Wang F, Zhang XZ (2011) Permian bimodal volcanism in the Zhangguangcai Range of eastern Heilongjiang Province, NE China: zircon U–Pb–Hf isotopes and geochemical evidence. J Asian Earth Sci 41:119–132

Murphy JB (2007) Arc magmatism II: geochemical and isotopic characteristics. Geosci Can 34:7–35

Patiño Douce AE (1995) Experimental generation of hybrid silicic melts by reaction of high-Al basalt with metamorphic rocks. J Geophys Res 100:15623–15639

Patiño Douce AE (1999) What do experiments tell us about the relative contributions of crust and mantle to the origin of granitic magmas? In: Castro A, Fernandez C, Vigneresse JL (eds) Understanding granites: integrating new and classical techniques. Geological Society of London Special Publication 168:55–75

Patiño Douce AE, Beard JS (1995) Dehydration-melting of biotite gneiss and quartz amphibolite from 3 to 15 kbar. J Petrol 36:707–738

Pearce JA (1996) Source and settings of granitic rocks. Episodes 19:120–125

Pearce JA, Harris NBW, Tindle AG (1984) Trace element discrimination diagrams for the tectonic interpretation of granitic rocks. J Petrol 25:956–983

Peccerillo A, Taylor AR (1976) Geochemistry of Eocene calc-alkaline volcanic rocks from the Kastamonu area, Northern Turkey. Contrib Miner Petrol 58:63–81

Pei FP, Xu WL, Yang DB, Zhao QG, Liu XM, Hu ZC (2007) Zircon U–Pb geochronology of basement metamorphic rocks in the Songliao basin. Chin Sci Bull 52:942–948

Rapp RP, Watson EB (1995) Dehydration melting of metabasalt at 8–32 kbar: implications for continental growth and crust–mantle recycling. J Petrol 36:891–931

Rapp RP, Shimizu N, Norman MD, Applegate GS (1999) Reaction between slab-derived melts and peridotite in the mantle wedge: experimental constraints at 3.8 GPa. Chem Geol 160:335–356

Ren LD, Wang YB, Yang CH, Zhao ZR, Guo JJ, Gao HL (2012) Two types of metamorphism and their relationships with granites in the Mashan Complex. Acta Petrologica Sinica 28(9):2855–2865 **(in Chinese with English abstract)**

Roberts MP, Clemens JD (1993) Origin of high-potassium calc-alkaline, I-type granitoids. Geology 21:825–828

Rogers G, Hawkesworth CJ (1989) A geochemical traverse across the North Chilean Andes: evidence for crustal generation from the mantle wedge. Earth Planet Sci Lett 91:271–285

Safonova IY, Santosh M (2014) Accretionary complexes in the Asia-Pacific region: tracing archives of ocean plate stratigraphy and tracking mantle plumes. Gondwana Res 25:126–158

Safonova IY, Utsunomiya A, Kojima S, Naka ES, Koizumi K, Tomurtogoo O, Filippov AN (2009) Pacific superplume-related oceanic basalts hosted by accretionary complexes of Central Asia, Russian Far East and Japan. Gondwana Res 16:587–608

Safonova IY, Seltmann R, Kroener A, Gladkochub D, Schulmann K, Xiao W, Kim T, Komiya T, Sun M (2011) A new concept of continental construction in the Central Asian Orogenic Belt (compared to actualistic examples from the Western Pacific). Episodes 34:186–194

Sano S (1992) Neodymium isotopic compositions of Silurian Yakuno metagabbros. J Mineral Petrol Econ Geol 87:272–282

Scherer E, Munker C, Mezger K (2001) Calibration of the Lutetium-hafnium clock. Science 293:683–687

Shellnutt G, Dostal J (2015) Granodiorites of the South Mountain Batholith (Nova Scotia, Canada) derived by partial melting of Avalonia granulite rocks beneath the Meguma terrane: implications for the heat source of the Late Devonian granites of the Northern Appalachians. Tectonophysics 655:206–212

Sivell WJ, Waterhouse JB (1988) Petrogenesis of Gympie Group Volcanics—evidence for remnants of an early Permian volcanic arc in Eastern Australia. Lithos 21:81–95

Sun SS, McDonough WF (1989) Chemical and isotopic systematics of oceanic basalts: Implications for mantle composition and processes. In: Saunders AD, Norry MJ (eds) Magmatism in Ocean Basins. Geological Society of Special Publication, London, pp 313–345

Sun MD, Xu YG, Wilde SA, Chen HL, Yang SF (2015a) The Permian Dongfanghong island-arc gabbro of the Wandashan Orogen, NE China: implications for Paleo-Pacific subduction. Tectonophysics 659:122–136

Sun MD, Xu YG, Wilde SA, Chen HL (2015b) Provenance of Cretaceous trench slope sediments from the Mesozoic Wandashan Orogen, NE China: implications for determining ancient drainage systems and tectonics of the Paleo-Pacific. Tectonics. doi:10.1002/2015TC003870

Suzuki N, Kojima S, Kano H, Yamakita S, Misaki A, Ehiro M, Otoh Sh, Kurihara T, Aoyama M (2005) Permian radiolarian faunas from chert in the Khabarovsk Complex, Far East Russia, and the age of each lithological unit of the Khabarovsk complex. J Paleontol 79:686–700

Sylvester PJ (1998) Post-collisional strongly peraluminous granites. Lithos 45:29–44

Wang Y, Zhang FQ, Zhang DW, Miao LC, Li TS, Xie HQ, Meng QR, Liu DY (2006) Zircon SHRIMP U–Pb dating of meta-diorite from the basement of the Songliao Basin and its geological significance. Chin Sci Bull 51:1877–1883

Wang F, Xu WL, Xu YG, Gao FH, Ge WC (2015) Late Triassic bimodal igneous rocks in eastern Heilongjiang Province, NE China: implications for the initiation of subduction of the Paleo-Pacific Plate beneath Eurasia. J. Asian Earth Sci. 97(Part B):406–423

Wei HY (2012) Geochronology and petrogenesis of granitoids in Yichun-Hegang, Area. Jilin University (in Chinese with English abstract), Heilongjiang Province

Whalen JB, Syme EC, Stern RA (1999) Geochemical and Nd isotopic evolution of Paleoproterozoic arc-type granitoid magmatism in the Flin Flon Belt, Trans-Hudson orogen, Canada. Can J Earth Sci 36:227–250

Wilde SA, Dorsett-Bain HL, Lennon RG (1999) Geological setting and controls on the development of graphite, sillimanite and phosphate mineralisation within the Jiamusi Massif: an exotic fragment of Gondwanaland located in North-Eastern China? Mineralisation in Gondwana, Dissanayake CB (ed). Gondwana Res 2:21–46

Wilde SA, Zhang XZ, Wu FY (2000) Extension of a newly-identified 500 Ma metamorphic terrain in northeast China: further U–Pb SHRIMP dating of the Mashan complex, Heilongjiang Province, China. Tectonophysics 328:115–130

Wilde SA, Wu FY, Zhang XZ (2003) Late Pan-African magmatism in northeastern China: SHRIMP U–Pb zircon evidence for igneous ages from the Mashan Complex. Precambr Res 122:311–327

Wilde SA, Wu FY, Zhao GC (2010) The Khanka Block, NE China, and its significance to the evolution of the Central Asian Orogenic Belt and continental accretion. In: Kusky TM, Zhai MG, Xiao WJ (eds) The evolved continents: understanding processes of continental growth: Geological Society of London, Special Publication, 338, pp 117–137

Wilson W (1989) Igneous petrogenesis. Unwin Hyman, London 327–373

Windley BF, Alexeiev D, Xiao WJ, Kröner A, Badarch G (2007) Tectonic model for accretion of the Central Asian Orogenic Belt. J Geol Soc Lond 164:31–47

Wu FY, Jahn BM, Wilde SA, Sun DY (2000) Phanerozoic crustal growth: U–Pb and Sr–Nd isotopic evidence from the granites in northeastern China. Tectonophysics 328:89–113

Wu FY, Wilde SA, Sun DY (2001) Zircon SHRIMP ages of gneissic granites in Jiamusi Massif, northeastern China. Acta Petrologica Sinica 17:443–452 **(in Chinese with English abstract)**

Wu FY, Sun DY, Li HM, Jahn BM, Wilde SA (2002) A-type granites in northeastern China: age and geochemical constraints on their petrogenesis. Chem Geol 187:143–173

Wu FY, Jahn BM, Wilde SA, Lo CH, Yui TF, Lin Q, Ge WC, Sun DY (2003) Highly fractionated I-type granites in NE China (II): isotopic geochemistry and implications for crustal growth in the Phanerozoic. Lithos 67:191–204

Wu FY, Yang YH, Xie LW, Yang JH, Xu P (2006) Hf isotopic compositions of the standard zircons in U–Pb geochronology. Chem Geol 234:105–126

Wu FY, Yang JH, Lo CH, Wilde SA, Sun DY, Jahn BM (2007) The Heilongjiang Group: a Jurassic accretionary complex in the Jiamusi Massif at the western Pacific margin of northeastern China. Isl Arc 16:156–172

Wu FY, Sun DY, Ge WC, Zhang YB, Grant ML, Wilde SA, Jahn BM (2011) Geochronology of the Phanerozoic granitoids in northeastern China. J Asian Earth Sci 41:1–30

Wyllie PJ, Wolf MB, Vander Laan SR (1996) Conditions for formation of tonalites and trondhjemites: magma sources and products. In: De Wit MJ, Ashwal LD (eds) Tectonic evolution of greenstone belts. Oxford University Press, pp 258–267

Xiao WJ, Zhang LC, Qin KZ, Sun S, Li JY (2004) Paleozoic accretionary and collisional tectonics of the eastern Tienshan (China): implications for the continental growth of Central Asia. Am J Sci 304:370–395

Yang JZ, Qiu HJ, Sun JP, Zhang XZ (1998) Yuejinshan complex and its tectonic significance. J Chang Univ Sci Technol 28(4):380–385 **(in Chinese with English abstract)**

Yang JH, Wu FY, Wilde SA, Zhao GC (2008) Petrogenesis and geodynamics of Late Archean magmatism in eastern Hebei, eastern North China Craton: geochronological, geochemical and Nd–Hf isotopic evidence. Precambr Res 167:125–149

Yang H, Zhang YL, Chen HJ, Ge WC (2012) Zircon U–Pb ages of Khanka Lake granitic complex and its geological implication. Glob Geol 31:621–630 **(in Chinese with English abstract)**

Yang H, Ge WC, Zhao GC, Dong Y, Bi JH, Wang ZH, Yu JJ, Zhang YL (2014) Geochronology and geochemistry of Late Pan-African intrusive rocks in the Jiamusi-Khanka Block, NE China: petrogenesis and geodynamic implications. Lithos 208–209:220–236

Yang H, Ge WC, Zhao GC, Yu JJ, Zhang YL (2015a) Early Permian-Late Triassic granitic magmatism in the Jiamusi-Khanka Massif, eastern segment of the Central Asian Orogenic Belt and its implications. Gondwana Res 27:1509–1533

Yang H, Ge WC, Zhao GC, Dong Y, Xu WL, Wang ZH, Ji Z, Yu JJ (2015b) Late Triassic intrusive complex in the Jidong region, Jiamusi-Khanka Block, NE China: geochemistry, zircon U–Pb ages, Lu–Hf isotopes, and implications for magma mingling and mixing. Lithos 224–225:143–159

Yu JJ, Hou XG, Ge WC, Zhang YL, Liu JC (2013a) Magma Mixing Genesis of the Early Permian Liulian pluton at the northeastern margin of the Jiamusi massif in NE China: evidences from petrography, geochronology and geochemistry. Acta Petrologica Sinica 29(9):2971–2986 **(in Chinese with English abstract)**

Yu JJ, Wang F, Xu WL, Gao FH, Tang J (2013b) Late Permian tectonic evolution at the southeastern margin of the Songnen-Zhangguangcai Range Massif, NE China: constraints from geochronology and geochemistry of granitoids. Gondwana Res 24(2):635–647

Zhang KJ (1997) North and South China collision along the eastern and southern North China margins. Tectonophysics 270:145–156

Zhang KW, Shao JA, Tang KD, Zhang Q, Li XY (1997) The geochemical characteristics and the geological significance of green-schists in Yuejinshan Group east Heilongjiang Province, China. Acta Petrologica Sinica 13(2):168–172 **(in Chinese with English abstract)**

Zhang L, Li QG, Shi XJ, Tong Y, Hou JY, Zhang JJ, Wang T (2013) Zircon U–Pb age and geochemistry of the Permian Yongqing granodiorite intrusion in the Jiamusi massif of Northeast China and their implications. Acta Petrologica Et Mineralogica 32(6):1022–1036 **(in Chinese with English abstract)**

Zhao GC (2015) Jiangnan Orogen in South China: Developing from divergent double subduction. Gondwana Res 27:1173–1180

Zhou JB, Wilde SA (2013) The crustal accretion history and tectonic evolution of the NE China segment of the Central Asian Orogenic Belt. Gondwana Res 23(4):1365–1377

Zhou JB, Wilde SA, Zhang XZ, Zhao GC, Zheng CQ, Wang YJ, Zhang XH (2009) The onset of Pacific margin accretion in NE China: evidence from the Heilongjiang high-pressure metamorphic belt. Tectonophysics 478:230–246

Zhou JB, Wilde SA, Zhao GC, Zhang XZ, Zheng CQ, Wang H (2010) New SHRIMP U–Pb zircon ages from the Heilongjiang high-pressure belt: constraints on the Mesozoic evolution of NE China. Am J Sci 310(9):1024–1053

Zhou JB, Cao JL, Wilde SA, Zhao GC, Zhang J, Wang B (2014) Paleo-Pacific subduction-accretion: evidence from Geochemical and U–Pb zircon dating of the Nadanhada accretionary complex, NE China. Tectonics 33:2444–2466

Zhu CY, Zhao GC, Sun M, Liu Q, Han YG, Hou WZ, Zhang XR, Eizenhofer PR (2015) Geochronology and geochemistry of the Yilan blueschists in the Heilongjiang Complex, northeastern China and tectonic implications. Lithos 216:241–253

Zhu CY, Zhao GC, Sun M, Eizenhofer PR, Liu Q, Zhang XR, Han YG, Hou WZ (2016) Geochronology and geochemistry of the Yilan greenschists and amphibolites in the Heilongjiang complex, northeastern China and tectonic implications. Gondwana Res. doi:10.1016/j.gr.2016.02.001